ESAIM: M2AN 56 (2022) 1327–1360
https://doi.org/10.1051/m2an/2022041

ESAIM: Mathematical Modelling and Numerical Analysis
www.esaim-m2an.org

WELL-BALANCED POSITIVITY PRESERVING ADAPTIVE MOVING MESH CENTRAL-UPWIND SCHEMES FOR THE SAINT-VENANT SYSTEM

Alexander Kurganov[1,*], Zhuolin Qu[2] and Tong Wu[2]

Abstract. We extend the adaptive moving mesh (AMM) central-upwind schemes recently proposed in Kurganov *et al.* [*Commun. Appl. Math. Comput.* **3** (2021) 445–479] in the context of one- (1-D) and two-dimensional (2-D) Euler equations of gas dynamics and granular hydrodynamics, to the 1-D and 2-D Saint-Venant system of shallow water equations. When the bottom topography is nonflat, these equations form hyperbolic systems of balance laws, for which a good numerical method should be capable of preserving a delicate balance between the flux and source terms as well as preserving the nonnegativity of water depth even in the presence of dry or almost dry regions. Therefore, in order to extend the AMM central-upwind schemes to the Saint-Venant systems, we develop special positivity preserving reconstruction and evolution steps of the AMM algorithms as well as special corrections of the solution projection step in (almost) dry areas. At the same time, we enforce the moving mesh to be structured even in the case of complicated 2-D computational domains. We test the designed method on a number of 1-D and 2-D examples that demonstrate robustness and high resolution of the proposed numerical approach.

Mathematics Subject Classification. 65M50, 76M12, 65M08, 86-08, 35L65, 35L67.

Received September 7, 2021. Accepted April 21, 2022.

1. Introduction

We consider the Saint-Venant system of shallow water equations, which was first introduced in [10] and is widely used to model water flow in rivers, canals and coastal areas as well as in atmospheric sciences and oceanography. In the one-dimensional (1-D) case the studied system reads as

$$\begin{pmatrix} h \\ hu \end{pmatrix}_t + \begin{pmatrix} hu \\ hu^2 + \dfrac{g}{2}h^2 \end{pmatrix}_x = \begin{pmatrix} 0 \\ -ghB_x \end{pmatrix}, \tag{1.1}$$

Keywords and phrases. Adaptive moving mesh methods, Saint-Venant systems of shallow water equations, finite-volume methods, well-balanced methods, positivity preserving methods, central-upwind schemes, moving mesh differential equations.

[1] Department of Mathematics, SUSTech International Center for Mathematics and Guangdong Provincial Key Laboratory of Computational Science and Material Design, Southern University of Science and Technology, Shenzhen 518055, P.R. China

[2] Department of Mathematics, The University of Texas at San Antonio, San Antonio, TX 78249, USA.

*Corresponding author: alexander@sustech.edu.cn

© The authors. Published by EDP Sciences, SMAI 2022

This is an Open Access article distributed under the terms of the Creative Commons Attribution License (https://creativecommons.org/licenses/by/4.0), which permits unrestricted use, distribution, and reproduction in any medium, provided the original work is properly cited.

where $h(x,t)$ is the water depth, $u(x,t)$ is the velocity, $B(x)$ is the bottom topography, and g is the constant gravitational acceleration. The two-dimensional (2-D) Saint-Venant system is

$$\begin{pmatrix} h \\ hu \\ hv \end{pmatrix}_t + \begin{pmatrix} hu \\ hu^2 + \frac{g}{2}h^2 \\ huv \end{pmatrix}_x + \begin{pmatrix} hv \\ huv \\ hv^2 + \frac{g}{2}h^2 \end{pmatrix}_y = \begin{pmatrix} 0 \\ -ghB_x \\ -ghB_y \end{pmatrix}, \tag{1.2}$$

where $h(x,y,t)$ is the water depth, $u(x,y,t)$ and $v(x,y,t)$ are the x- and y-velocities, and $B(x,y)$ is the bottom topography.

Development of accurate, efficient and robust numerical methods for the systems (1.1) and (1.2) is an important and challenging problem due to several reasons. First, these systems admit nonsmooth solution, which, in the case of discontinuous bottom topography B, may not be unique. Second, it is very important to preserve a delicate balance between the flux and source terms since many practically relevant solutions are, in fact, small perturbations of the so-called "lake at rest" steady states:

$$w := h + B = \text{Const}, \quad u \equiv v \equiv 0,$$

where w is an equilibrium water surface variable (we say that a numerical method is well-balanced if it is capable of exactly preserving the "lake at rest" states). Third, in many practically important situations, one may need to deal with dry or almost dry areas and then it is crucial for the developed numerical method to preserve the nonnegativity of h.

In the past decades, many well-balanced and positivity preserving numerical methods for the Saint-Venant systems have been developed; see, *e.g.*, the review papers [16, 24] and references therein. In this paper, we focus on semi-discrete central-upwind schemes for (1.1) and (1.2), which were designed on a variety of fixed grids: uniform Cartesian [5, 17, 18], unstructured triangular [7], quadrilateral [21], and cell-vertex polygonal [3] ones. We follow the lines of [19] and construct an adaptive moving mesh (AMM) central-upwind scheme for the Saint-Venant systems (1.1) and (1.2). The AMM central-upwind schemes, which have been recently introduced in [19] for 1-D and 2-D hyperbolic systems of PDEs, are based on structural meshes, which are evolved in time according to the movimg mesh differential equations; we refer the reader to [1,8,9,13] for several examples of existing AMM algoritms. Our goal is to develop several techniques required to ensure that the resulting scheme is well-balanced and positivity preserving. In order to achieve this goal, we first generalize the 1-D well-balanced positivity preserving semi-discrete central-upwind scheme from [17] for the 1-D nonuniform grids and modify the 2-D well-balanced positivity preserving semi-discrete central-upwind scheme from [21] to evolve the solution over the structured quadrilateral meshes. In these schemes, second-order well-balanced quadratures for the geometric source terms are developed to ensure the well-balanced property. In order to preserve the positivity of the computed water depth, several measures are taken. First, we either make sure that the reconstructed values of the water surface stay above the corresponding values of the bottom topography or use the positivity preserving reconstructions for the water depth. Second, we use a draining time-step technique, originally proposed in [4], to ensure that the water depth remains positive during the evolution step. Third, we propose special corrections of the solution projection step in (almost) dry areas. We stress that the positivity preserving technique we develop here does not allow us to ensure the well-balanced property of the proposed AMM central-upwind schemes in the presence of dry areas. An alternative positivity preserving approach was proposed in [25,26], where a GRP AMM method on unstructured triangular meshes was introduced. In addition to preserving positivity of the water depth, this method is capable of ensuring the total water conservation, which is enforced by redistributing the conservation error. Such redistribution, however, may lead to a purely artificial appearance of water in dry areas and we prefer not to implement this technique in our AMM method. Finally, we stress that development of a well-balanced AMM method that can accurately handle wetting/drying interfaces and preserve both "lake at rest" and "dry lake" steady states still remains an open problem.

The paper is organized as follows. The proposed AMM algorithms are presented in Section 2. First, in Section 2.1, we introduce the second-order well-balanced and positivity preserving central-upwind scheme on

1-D nonuniform grids for the system (1.1). Then, in Section 2.2, we discuss the 1-D moving mesh equation and its discretization. We complete the description of the 1-D AMM algorithm in Section 2.3, where we introduce the 1-D conservative positivity preserving projection. In Section 2.4, we present the second-order well-balanced and positivity preserving central-upwind scheme on 2-D structured quadrilateral meshes for the system (1.2). We then design the 2-D AMM algorithm with the help of the 2-D moving mesh equation, which is discussed together with its discretization in Section 2.5, and a special 2-D conservative positivity preserving projection, which is introduced in Section 2.6. Finally, in Section 3, we demonstrate the performance of the proposed AMM algorithms through several 1-D and 2-D numerical examples.

2. Adaptive Moving Mesh central-upwind schemes

In this section, we present the AMM central-upwind schemes for the systems (1.1) and (1.2). The schemes are based on the 1-D and 2-D AMM central-upwind schemes introduced in [19]. They are constructed in two steps. Given the solution at a certain time level, it is first evolved to the new time level on a given mesh (see Sects. 2.1 and 2.4), which is updated at the end of the evolution step by solving the moving mesh differential equation (see Sects. 2.2 and 2.5). The solution is then projected in a conservative manner to the new finite-volume mesh (see Sects. 2.3 and 2.6).

We use the same notation as in [19], which is briefly reviewed in this paper for the sake of completeness.

2.1. One-dimensional semi-discrete scheme

We first rewrite the system (1.1) in terms of the water depth h and discharge $q := hu$:

$$\begin{pmatrix} h \\ q \end{pmatrix}_t + \begin{pmatrix} q \\ \dfrac{q^2}{h} + \dfrac{g}{2}h^2 \end{pmatrix}_x = \begin{pmatrix} 0 \\ -ghB_x \end{pmatrix}.$$

This system can be put into the vector form

$$\boldsymbol{U}_t + \boldsymbol{F}(\boldsymbol{U})_x = \boldsymbol{S}(\boldsymbol{U}, B) \tag{2.1}$$

with

$$\boldsymbol{U} := \begin{pmatrix} h \\ q \end{pmatrix}, \quad \boldsymbol{F}(\boldsymbol{U}, B) := \begin{pmatrix} q \\ \dfrac{q^2}{h} + \dfrac{g}{2}h^2 \end{pmatrix}, \quad \boldsymbol{S}(\boldsymbol{U}, B) := \begin{pmatrix} 0 \\ -ghB_x \end{pmatrix}. \tag{2.2}$$

We then apply the 1-D AMM central-upwind scheme from [19] to the system (2.1), (2.2). As mentioned in Section 1, we will need to develop the scheme that preserves the positivity of h and is well-balanced in the sense that it is capable of exactly preserving the "lake at rest" steady states ($w \equiv \text{Const}$, $q \equiv 0$).

Assume that the computational domain is covered with nonuniform cells $C_j = \left[x_{j-\frac{1}{2}}, x_{j+\frac{1}{2}}\right]$ of the size $\Delta x_j := x_{j+\frac{1}{2}} - x_{j-\frac{1}{2}}$ centered at $x_j := \left(x_{j-\frac{1}{2}} + x_{j+\frac{1}{2}}\right)/2$, and that at a certain time t, the cell averages of the computed solution,

$$\overline{\boldsymbol{U}}_j(t) \approx \frac{1}{\Delta x_j}\int_{C_j} \boldsymbol{U}(x,t)\,\mathrm{d}x,$$

are available. They are then evolved from time level t to $t + \Delta t$ using the semi-discrete central-upwind scheme on nonuniform grids from Section 2.1 of [19]:

$$\frac{\mathrm{d}}{\mathrm{d}t}\overline{\boldsymbol{U}}_j(t) = -\frac{\boldsymbol{H}_{j+\frac{1}{2}}(t) - \boldsymbol{H}_{j-\frac{1}{2}}(t)}{\Delta x_j} + \overline{\boldsymbol{S}}_j(t), \tag{2.3}$$

where the numerical fluxes are given by

$$\boldsymbol{H}_{j+\frac12}=\frac{a^+_{j+\frac12}\boldsymbol{F}^-_{j+\frac12}-a^-_{j+\frac12}\boldsymbol{F}^+_{j+\frac12}}{a^+_{j+\frac12}-a^-_{j+\frac12}}+\frac{a^+_{j+\frac12}a^-_{j+\frac12}}{a^+_{j+\frac12}-a^-_{j+\frac12}}\Big[\boldsymbol{U}^+_{j+\frac12}-\boldsymbol{U}^-_{j+\frac12}\Big]. \tag{2.4}$$

Here, $\boldsymbol{F}^\pm_{j+\frac12}=\boldsymbol{F}(\boldsymbol{U}^\pm_{j+\frac12})$, and the second component of the source term is approximated using the well-balanced quadrature developed in [17]:

$$\overline{S}^{(2)}_j=-g\,\frac{h^-_{j+\frac12}+h^+_{j-\frac12}}{2}\cdot\frac{B_{j+\frac12}-B_{j-\frac12}}{\Delta x_j}. \tag{2.5}$$

In (2.4) and (2.5), $\boldsymbol{U}^\pm_{j+\frac12}$ are the reconstructed one-sided point values of $\boldsymbol{U}\Big(x_{j+\frac12}\pm0,t\Big)$ (see Sect. 2.1.1), $B_{j\pm\frac12}:=B\Big(x_{j\pm\frac12}\Big)$, and $a^\pm_{j+\frac12}$ the one-sided local speeds of propagation (see Sect. 2.1.2).

Note that in (2.4), (2.5), all of the indexed quantities depend on t, but from now on, we will omit this dependence for the sake of brevity.

2.1.1. Positivity preserving reconstruction

We begin by following Section 2.1 of [19] and obtain the generalized minmod piecewise linear reconstruction of the water surface $w:=h+B$ and discharge $q:=hu$, which are used to evaluate $w^\pm_{j+\frac12}$ and $q^\pm_{j+\frac12}$. Unfortunately, for some j the obtained point values $w^\pm_{j+\frac12}$ may be smaller than the corresponding value $B_{j+\frac12}$, which would lead to negative point values of the water depth $h^\pm_{j+\frac12}:=w^\pm_{j+\frac12}-B_{j+\frac12}$. We therefore follow [17] and reconstruct h instead of w in potentially dry areas.

In this paper, the cell C_j is called "dry" if at least one of the following inequalities is satisfied:

$$\min\{\overline{w}_{j-1},\overline{w}_j,\overline{w}_{j+1}\}<\max_{x\in[x_{j-1},x_{j+1}]}B(x), \tag{2.6}$$

$$\overline{w}_j-\overline{B}_j<\delta, \tag{2.7}$$

where $\delta>0$ is a small parameter (we take $\delta=10^{-16}$ in all of the numerical experiments reported in Sect. 3) and $\overline{B}_j=\frac{1}{\Delta x_j}\int_{C_j}B(x)\,dx$, which should be numerically computed using a quadrature (in our numerical examples, we have used either the trapezoidal or Simpson's rule). All other cells are called "wet".

In "dry" cells, we use the piecewise linear positivity preserving reconstruction (described in [19], Sect. 2.1) of h based on the cell averages of water depth $\overline{h}_j:=\overline{w}_j-\overline{B}_j$. After computing $h^-_{j+\frac12}$ and $h^+_{j-\frac12}$ in the "dry" cell C_j, we obtain $w^+_{j-\frac12}:=h^+_{j-\frac12}+B_{j-\frac12}$ and $w^-_{j+\frac12}:=h^-_{j+\frac12}+B_{j+\frac12}$ there.

Remark 2.1. In practice, one may replace the condition (2.6) with its simplified version:

$$\min\{\overline{w}_{j-1},\overline{w}_j,\overline{w}_{j+1}\}<\max\Big\{\overline{B}_{j-1},B_{j-\frac12},\overline{B}_j,B_{j+\frac12},\overline{B}_{j+1}\Big\}, \tag{2.8}$$

which is much easier to check. We stress that the use of the simplified condition (2.8) does not guarantee positivity of the projected values of h (see the proof of Theorem 2.5 below), but negative h may appear only in a small number of cells located near the wet/dry interfaces. If this occurs, we reclassify these particular cells from "wet" to "dry" and reconstruct h instead of w in them.

2.1.2. Desingularization and one-sided local speeds

In order to avoid division by zero (or by a very small number), we follow [18] and desingularize the computation of the velocity point values needed to evaluate numerical fluxes in (2.4) by setting

$$u^\pm_{j+\frac12}=\frac{\sqrt{2}\,h^\pm_{j+\frac12}q^\pm_{j+\frac12}}{\sqrt{\Big(h^\pm_{j+\frac12}\Big)^4+\max\Big[\Big(h^\pm_{j+\frac12}\Big)^4,\varepsilon^4\Big]}}, \tag{2.9}$$

and then for consistency we modify the corresponding values of the discharge by recalculating

$$q^{\pm}_{j+\frac12}=h^{\pm}_{j+\frac12}\cdot u^{\pm}_{j+\frac12}.$$

In (2.9), ε is a small desingularization parameter, which we take to be equal to δ in (2.7).

Equipped with the values of $u^{\pm}_{j+\frac12}$ and $h^{\pm}_{j+\frac12}$, we estimate the one-sided local speeds of propagation needed in (2.4) as follows:

$$a^{+}_{j+\frac12}=\max\Big\{u^{+}_{j+\frac12}+\sqrt{gh^{+}_{j+\frac12}},\,u^{-}_{j+\frac12}+\sqrt{gh^{-}_{j+\frac12}},\,0\Big\},$$
$$a^{-}_{j+\frac12}=\min\Big\{u^{+}_{j+\frac12}-\sqrt{gh^{+}_{j+\frac12}},\,u^{-}_{j+\frac12}-\sqrt{gh^{-}_{j+\frac12}},\,0\Big\}.$$

2.1.3. Positivity preserving evolution

In order to guarantee the positivity of h during the evolution step, a draining time-step technique introduced in [4] is employed.

We first consider the forward Euler discretization of (2.3), the first component of which reads as

$$\overline{h}_j(t+\Delta t)=\overline{h}_j(t)-\Delta t\,\frac{H^{(1)}_{j+\frac12}-H^{(1)}_{j-\frac12}}{\Delta x_j},\tag{2.10}$$

where Δt is the time step constrained by the CFL condition:

$$\Delta t\,\max_j\left\{\frac{\max\Big\{\Big|a^{+}_{j-\frac12}\Big|,\Big|a^{-}_{j+\frac12}\Big|\Big\}}{\Delta x_j}\right\}\le\frac12.$$

We then denote by

$$\Delta t^{\rm drain}_j:=\frac{\Delta x_j\,\overline{h}_j(t)}{\max\Big(0,H^{(1)}_{j+\frac12}\Big)+\max\Big(0,-H^{(1)}_{j-\frac12}\Big)},$$

and replace (2.10) by

$$\overline{h}_j(t+\Delta t)=\overline{h}_j(t)-\frac{\Delta t_{j+\frac12}H^{(1)}_{j+\frac12}-\Delta t_{j-\frac12}H^{(1)}_{j-\frac12}}{\Delta x_j},$$

where the time step $\Delta t_{j+\frac12}$ is defined as:

$$\Delta t_{j+\frac12}=\min\big(\Delta t,\Delta t^{\rm drain}_i\big),\quad i=j+\frac12-\frac{\operatorname{sgn}\Big(H^{(1)}_{j+\frac12}\Big)}{2}.$$

The corresponding forward Euler step for $\overline{q}_j$ is

$$\overline{q}_j(t+\Delta t)=\overline{q}_j(t)-\frac{\Delta t_{j+\frac12}H^{(a,2)}_{j+\frac12}-\Delta t_{j-\frac12}H^{(a,2)}_{j-\frac12}}{\Delta x_j}-\Delta t\left(\frac{H^{(g,2)}_{j+\frac12}-H^{(g,2)}_{j-\frac12}}{\Delta x_j}-\overline{S}^{(2)}\right),$$

where the advective and gravitational parts of the fluxes are defined by

$$\begin{cases}H^{(a,2)}_{j+\frac12}=\dfrac{a^{+}_{j+\frac12}h^{-}_{j+\frac12}\Big(u^{-}_{j+\frac12}\Big)^2-a^{-}_{j+\frac12}h^{+}_{j+\frac12}\Big(u^{+}_{j+\frac12}\Big)^2}{a^{+}_{j+\frac12}-a^{-}_{j+\frac12}},\\[2ex] H^{(g,2)}_{j+\frac12}=g\dfrac{a^{+}_{j+\frac12}\Big(h^{-}_{j+\frac12}\Big)^2-a^{-}_{j+\frac12}\Big(h^{+}_{j+\frac12}\Big)^2}{2\Big(a^{+}_{j+\frac12}-a^{-}_{j+\frac12}\Big)}+\dfrac{a^{+}_{j+\frac12}a^{-}_{j+\frac12}}{a^{+}_{j+\frac12}-a^{-}_{j+\frac12}}\Big(q^{+}_{j+\frac12}-q^{-}_{j+\frac12}\Big).\end{cases}$$

It has been shown in [5] that in the case of uniform grid the resulting central-upwind scheme is both positivity preserving and well-balanced. The proof can be directly extended to the case of a nonuniform grid and the three-stage third-order strong stability preserving (SSP) Runge–Kutta method (see, *e.g.*, [11, 12]) as it can be written as a convex combination of forward Euler steps.

Remark 2.2. An alternative way to ensure the positivity of h during the time evolution is to use a more restrictive CFL condition, which we derive in Appendix C.1. This approach, however, will significantly affect the efficiency of the overall method as the size of time steps is to be reduced by a factor of about 3. We have carefully compared the numerical results obtained by both approaches and realized that using much smaller CFL number does not lead to any improvement in the quality of the computed solutions. Therefore, in all of the numerical examples reported in Section 3, we have used the draining time-step technique.

2.2. One-dimensional moving mesh equation

In this section, we briefly describe the 1-D moving mesh equation and its numerical solution algorithm; see Section 3.1 of [19] for details.

In addition to the computational domain $[a,b]$ covered by the nonuniform mesh $\left\{x_{j+\frac{1}{2}}\right\}$, we introduce the uniform logical mesh $\xi_{j+\frac{1}{2}} = j\Delta\xi, j = 0,\ldots,N$, with $\Delta\xi = 1/N$. Let us denote the one-to-one coordinate transformation from the logical domain to the computational one by

$$x = x(\xi), \quad \xi \in [0,1], \quad x(0) = a, \quad x(1) = b,$$

so that $x_{j+\frac{1}{2}} = x\left(\xi_{j+\frac{1}{2}}\right)$.

The mesh is distributed according to the following moving mesh equation (see, *e.g.*, [13] for a detailed derivation):

$$(\omega x_\xi)_\xi = 0, \quad \omega(\boldsymbol{U}) = 1 + \alpha\varphi(|D\boldsymbol{U}|), \tag{2.11}$$

where ω is a monitor function and D is a differential operator (see, *e.g.*, [2, 13, 23]). In this paper, we use $D\boldsymbol{U} = U^{(i)}_{\xi\xi}$ (for some component of $\boldsymbol{U}$), which is approximated using the second-order centered difference:

$$D\boldsymbol{U}_j = \left(U^{(i)}_{\xi\xi}\right)_j = \frac{\overline{U}^{(i)}_{j+1} - 2\overline{U}^{(i)}_j + \overline{U}^{(i)}_{j-1}}{(\Delta\xi)^2}.$$

The function φ in (2.11) is a smoothing filter designed as follows. We first compute $\varphi^0_j = |D\boldsymbol{U}_j|$, and then smooth φ^0_j out by averaging over the neighboring cells for each j for a prescribed number of iterations, that is, we introduce

$$\varphi^{\ell+1}_j = \frac{1}{4}\left(\varphi^\ell_{j+1} + 2\varphi^\ell_j + \varphi^\ell_{j-1}\right), \quad \ell = 0,1,\ldots,m-1,$$

and then set $(\varphi(|D\boldsymbol{U}|))_j := \varphi^m_j$, which is used in (2.11). In our numerical experiments, we have taken $m = 4$.

Finally, α in (2.11) is the intensity parameter employed to control the mesh concentration: the use of larger values of α leads to the higher concentration of grid points in the "rough" areas. We follow [14] and choose α to be

$$\alpha = \left(\frac{1-\beta}{\beta(b-a)}\int_a^b \varphi(|D\boldsymbol{U}|)\,\mathrm{d}x\right)^{-1},$$

where $\beta \in (0,1)$ is a prescribed fraction of mesh points to be concentrated in the "rough" areas of the computed solution.

Equipped with the monitor function ω, we discretize the moving mesh equation (2.11) using the centered difference approximation, which results in the following linear algebraic system for the mesh points locations:

$$\begin{cases} x_{\frac{1}{2}} = a, \\ \omega_{j+1}\Big(x_{j+\frac{3}{2}} - x_{j+\frac{1}{2}}\Big) - \omega_j\Big(x_{j+\frac{1}{2}} - x_{j-\frac{1}{2}}\Big) = 0, \quad j = 1, \dots N-1, \\ x_{N+\frac{1}{2}} = b. \end{cases}$$

We numerically solve this system using the Jacobi iterations combined with the mesh relaxation procedure needed to ensure that the mesh does not get distracted during the iterations. Denoting by $x^{\nu}_{j+\frac{1}{2}}$ the grid nodes in the beginning of the $(\nu+1)$-th iteration step (with the initial guess $x^{0}_{j+\frac{1}{2}}$ being the grid nodes from the previous evolution step), we take one Jacobi sweep

$$x^{*}_{j+\frac{1}{2}} = \frac{\omega^{\nu}_{j+1}x^{\nu}_{j+\frac{3}{2}} + \omega^{\nu}_{j}x^{\nu}_{j-\frac{1}{2}}}{\omega^{\nu}_{j+1} + \omega^{\nu}_{j}} \quad j = 1, \dots N-1,$$

where ω^{ν}_{j} is the values of the monitor function ω at the grid point $x = x^{\nu}_{j}$ computed using the cell averages $\Big\{\overline{\boldsymbol{U}}^{\,\nu}_{j}\Big\}$. This results in the grid $\Big\{x^{*}_{j+\frac{1}{2}}\Big\}$, which is then relaxed by setting

$$x^{\nu+1}_{j+\frac{1}{2}} = \frac{1}{2}\Big(x^{\nu}_{j+\frac{1}{2}} + x^{*}_{j+\frac{1}{2}}\Big), \quad j = 1, \dots N-1, \tag{2.12}$$

which implies

$$x^{\nu}_{j} = \frac{1}{2}\Big(x^{\nu}_{j-\frac{1}{2}} + x^{\nu}_{j+\frac{1}{2}}\Big) \le x^{\nu+1}_{j+\frac{1}{2}} \le \frac{1}{2}\Big(x^{\nu}_{j+\frac{1}{2}} + x^{\nu}_{j+\frac{3}{2}}\Big) = x^{\nu}_{j+1}, \tag{2.13}$$

and thus $x^{\nu+1}_{j+\frac{1}{2}} \in \Big(x^{\nu+1}_{j-\frac{1}{2}}, x^{\nu+1}_{j+\frac{3}{2}}\Big)$, which means that the logical structure of the mesh does not change.

Remark 2.3. One can set up a stopping criterion for the iteration (2.12), for instance, the iterations should stop as soon as $\max_j\Big\{\Big|x^{\nu+1}_{j+\frac{1}{2}} - x^{\nu}_{j+\frac{1}{2}}\Big|\Big\} < tol$ for a given $tol > 0$. In practice, however, the mesh does not typically change much in one evolution time step. We therefore improve the efficiency of the resulting AMM method by stopping the iteration process after several iterations. In all of our numerical experiments, the upper bound on the number of iterations has been set to 4.

Remark 2.4. In order to avoid the appearances of excessively small cells, which would lead to severe time step restrictions, we modify the mesh movement as follows. If $\Big|x^{\nu+1}_{j+\frac{1}{2}} - x^{\nu+1}_{j-\frac{1}{2}}\Big| < \Delta x_{\min}$, where $\Delta x_{\min}$ is the smallest allowed cell size, then we locally freeze the movement of the mesh by setting $x^{\nu+1}_{j\pm\frac{1}{2}} = x^{\nu}_{j\pm\frac{1}{2}}$, and in the next iteration of moving mesh process, we set $\varphi^{0}_{j-1} = 0$, $\varphi^{0}_{j} = 0$ and $\varphi^{0}_{j+1} = 0$ to reduce the mesh concentration nearby. In all of the numerical examples, we have set $\Delta x_{\min} = 0.1\Delta x_{\text{unif}}$, where Δx_{unif} is the size of cells of the corresponding uniform mesh, which contains precisely the same total number of cells as used in the AMM computations.

2.3. One-dimensional conservative positivity preserving projection

After obtaining the new mesh, we project the solution from the cells $C^{\nu}_{j} := \Big[x^{\nu}_{j-\frac{1}{2}}, x^{\nu}_{j+\frac{1}{2}}\Big]$ to the new cells $C^{\nu+1}_{j} := \Big[x^{\nu+1}_{j-\frac{1}{2}}, x^{\nu+1}_{j+\frac{1}{2}}\Big]$.

Let $\overline{\boldsymbol{U}}^{\,\nu}_{j}$ and $\overline{\boldsymbol{U}}^{\,\nu+1}_{j}$ be the cell averages over the cells C^{ν}_{j} and $C^{\nu+1}_{j}$, respectively, and denote the mesh shift by $\mu^{\nu+\frac{1}{2}}_{j+\frac{1}{2}} := x^{\nu+1}_{j+\frac{1}{2}} - x^{\nu}_{j+\frac{1}{2}}$. The conservative solution projection step from [22] is given by

$$\Delta x^{\nu+1}_{j}\overline{\boldsymbol{U}}^{\,\nu+1}_{j} = \Delta x^{\nu}_{j}\,\overline{\boldsymbol{U}}^{\,\nu}_{j} + \mu^{\nu+\frac{1}{2}}_{j+\frac{1}{2}}\boldsymbol{U}^{\nu}_{j+\frac{1}{2}} - \mu^{\nu+\frac{1}{2}}_{j-\frac{1}{2}}\boldsymbol{U}^{\nu}_{j-\frac{1}{2}},$$

where

$$\boldsymbol{U}^{\nu}_{j+\frac{1}{2}}:=\begin{cases}\boldsymbol{U}^{+}_{j+\frac{1}{2}}, & \text{if } \mu^{\nu+\frac{1}{2}}_{j+\frac{1}{2}}>0,\\ \boldsymbol{U}^{-}_{j+\frac{1}{2}}, & \text{if } \mu^{\nu+\frac{1}{2}}_{j+\frac{1}{2}}<0,\end{cases} \tag{2.14}$$

and $\boldsymbol{U}^{\pm}_{j+\frac{1}{2}}$ are the point values reconstructed over the grid C^{ν}_{j} as described in Section 2.1.1.

In particular, this projection step for the water surface variable w reads as

$$\Delta x^{\nu+1}_{j}\overline{w}^{\nu+1}_{j}=\Delta x^{\nu}_{j}\,\overline{w}^{\nu}_{j}+\mu^{\nu+\frac{1}{2}}_{j+\frac{1}{2}}w^{\nu}_{j+\frac{1}{2}}-\mu^{\nu+\frac{1}{2}}_{j-\frac{1}{2}}w^{\nu}_{j-\frac{1}{2}}. \tag{2.15}$$

We note that this projection step preserves "lake at rest" steady states, for which $\overline{w}_j=w^{\pm}_{j\pm\frac{1}{2}}=\overline{w}$ for all j, and thus (2.15) reduces to

$$\Delta x^{\nu+1}_{j}\,\overline{w}^{\nu+1}_{j}=\Delta x^{\nu}_{j}\,\overline{w}+\left(x^{\nu+1}_{j+\frac{1}{2}}-x^{\nu}_{j+\frac{1}{2}}\right)\overline{w}-\left(x^{\nu+1}_{j-\frac{1}{2}}-x^{\nu}_{j-\frac{1}{2}}\right)\overline{w}=\Delta x^{\nu+1}_{j}\,\overline{w}.$$

We also note that the total amount of w after completion of this projection step is conserved, but the total amount of h is not conserved, since, in general,

$$\sum_j\overline{B}^{\nu}_{j}\Delta x^{\nu}_{j}\neq\sum_j\overline{B}^{\nu+1}_{j}\Delta x^{\nu+1}_{j},$$

where

$$\overline{B}^{\nu}_{j}\approx\frac{1}{\Delta x^{\nu}_{j}}\int_{C^{\nu}_{j}}B(x)\,\mathrm{d}x\quad\text{and}\quad\overline{B}^{\nu+1}_{j}\approx\frac{1}{\Delta x^{\nu+1}_{j}}\int_{C^{\nu+1}_{j}}B(x)\,\mathrm{d}x \tag{2.16}$$

are approximations of the cell averages of B, computed by a proper numerical quadrature. As one can expect, the use of a higher-order quadrature may help to reduce the conservation error. In the numerical experiments reported in Section 3, we have compared the results obtained using the trapezoidal and Simpson's rules and clearly seen the advantage of the higher-order quadrature.

The projection step (2.15), however, cannot be used in the "dry" areas, since one of the following may happen:

- appearance of negative water depth, that is, $\overline{w}^{\nu+1}_{j}<\overline{B}^{\nu+1}_{j}$ for some j;
- artificial propagation of water into dry areas, that is, $\overline{w}^{\nu+1}_{j}>\overline{B}^{\nu+1}_{j}$ for j located in the totally dry area (far away from the wetting/drying interface), where $\overline{w}^{\nu+1}_{j}$ must be equal to $\overline{B}^{\nu+1}_{j}$.

We therefore replace the projection step (2.15) with

$$\Delta x^{\nu+1}_{j}\,\overline{w}^{\nu+1}_{j}=\Delta x^{\nu}_{j}\,\overline{w}^{\nu}_{j}+\mu^{\nu+\frac{1}{2}}_{j+\frac{1}{2}}\widetilde{w}^{\nu}_{j+\frac{1}{2}}-\mu^{\nu+\frac{1}{2}}_{j-\frac{1}{2}}\widetilde{w}^{\nu}_{j-\frac{1}{2}}+B^{\mathrm{corr}}_{j}, \tag{2.17}$$

where

$$\widetilde{w}^{\nu}_{j+\frac{1}{2}}:=\begin{cases}w^{\nu}_{j+\frac{1}{2}}, & \text{if } C^{\nu}_{j} \text{ is "wet" and } \mu^{\nu+\frac{1}{2}}_{j+\frac{1}{2}}\le 0 \text{ or } C^{\nu}_{j+1} \text{ is "wet" and } \mu^{\nu+\frac{1}{2}}_{j+\frac{1}{2}}\ge 0,\\ h^{\nu}_{j+\frac{1}{2}}+\overline{B}^{\nu+\frac{1}{2}}_{j+\frac{1}{2}}, & \text{otherwise.}\end{cases}$$

Here, $w^{\nu}_{j+\frac{1}{2}}$ and $h^{\nu}_{j+\frac{1}{2}}$ are determined using (2.14) and

$$\overline{B}^{\nu+\frac{1}{2}}_{j+\frac{1}{2}}\approx\frac{1}{\mu^{\nu+\frac{1}{2}}_{j+\frac{1}{2}}}\int_{x^{\nu}_{j+\frac{1}{2}}}^{x^{\nu+1}_{j+\frac{1}{2}}}B(x)\,\mathrm{d}x \tag{2.18}$$

is an approximation of the average of B over the interval $\left[x^{\nu}_{j+\frac12},x^{\nu+1}_{j+\frac12}\right]$ or $\left[x^{\nu+1}_{j+\frac12},x^{\nu}_{j+\frac12}\right]$ depending on whether $x^{\nu+1}_{j+\frac12}>x^{\nu}_{j+\frac12}$ or $x^{\nu}_{j+\frac12}>x^{\nu+1}_{j+\frac12}$. Finally, the "dry" cell correction term $B^{\rm corr}_j$ is defined as

$$B^{\rm corr}_j:=\begin{cases}0, & \text{if } C_j \text{ is "wet"},\\ \Delta x^{\nu+1}_j\overline{B}^{\nu+1}_j-\left[\Delta x^{\nu}_j\overline{B}^{\nu}_j+\mu^{\nu+\frac12}_{j+\frac12}\overline{B}^{\nu+\frac12}_{j+\frac12}-\mu^{\nu+\frac12}_{j-\frac12}\overline{B}^{\nu+\frac12}_{j-\frac12}\right], & \text{otherwise.}\end{cases}\tag{2.19}$$

We note that the magnitude of $B^{\rm corr}_j$ is determined by the accuracy of the quadratures used to approximate the integrals in (2.16) and (2.18). Indeed, assuming that these integrals are evaluated using a quadrature of order p, we have

$$\begin{aligned}&\Delta x^{\nu+1}_j\overline{B}^{\nu+1}_j-\left[\Delta x^{\nu}_j\overline{B}^{\nu}_j+\mu^{\nu+\frac12}_{j+\frac12}\overline{B}^{\nu+\frac12}_{j+\frac12}-\mu^{\nu+\frac12}_{j-\frac12}\overline{B}^{\nu+\frac12}_{j-\frac12}\right]\\&\quad=\int_{x^{\nu+1}_{j-\frac12}}^{x^{\nu+1}_{j+\frac12}}B(x)\,{\rm d}x-\left[\int_{x^{\nu}_{j-\frac12}}^{x^{\nu}_{j+\frac12}}B(x)\,{\rm d}x+\int_{x^{\nu}_{j+\frac12}}^{x^{\nu+1}_{j+\frac12}}B(x)\,{\rm d}x-\int_{x^{\nu}_{j-\frac12}}^{x^{\nu+1}_{j-\frac12}}B(x)\,{\rm d}x\right]+\mathcal{O}\big(\Delta^{p+1}\big)=\mathcal{O}\big(\Delta^{p+1}\big),\end{aligned}$$

where $\Delta:=\max\Big\{\Delta x^{\nu},\Delta x^{\nu+1},\mu^{\nu+\frac12}_{j-\frac12},\mu^{\nu+\frac12}_{j+\frac12}\Big\}$.

We now state the positivity preserving property of the described projection step.

Theorem 2.5. *The projection step (2.17)–(2.19) preserves the positivity of $\overline{h}_j$, namely,*

$$\overline{w}^{\nu+1}_j\ge\overline{B}^{\nu+1}_j,\quad\forall j,\tag{2.20}$$

provided $\overline{w}^{\nu}_j\ge\overline{B}^{\nu}_j$, $\forall j$ and the integrals in (2.16) and (2.18) are evaluated exactly.

The proof of this important theorem is quite technical and provided in Appendix A.

Remark 2.6. The proof of Theorem 2.5 is still true if the integrals in (2.16) are computed by a numerical quadrature with nonnegative weights (for example, the trapezoidal and Simpson's rules, which have been used in our numerical experiments). We only need to assume that the integral in (2.18) is computed exactly. However, in our numerical experiments, we have used either the trapezoidal or Simpson's rule and $\overline{w}^{\nu+1}_j-\overline{B}^{\nu+1}_j$ always remained positive.

2.4. Two-dimensional semi-discrete scheme

Similarly to the 1-D case, we rewrite the system (1.2) in terms of water depth h and discharges $q^x:=hu$ and $q^y:=hv$:

$$\begin{pmatrix}h\\q^x\\q^y\end{pmatrix}_t+\begin{pmatrix}q^x\\\dfrac{(q^x)^2}{h}+\dfrac{g}{2}h^2\\\dfrac{q^xq^y}{h}\end{pmatrix}_x+\begin{pmatrix}q^y\\\dfrac{q^xq^y}{h}\\\dfrac{(q^y)^2}{h}+\dfrac{g}{2}h^2\end{pmatrix}_y=\begin{pmatrix}0\\-ghB_x\\-ghB_y\end{pmatrix}.$$

This system can be put into the vector form

$$\boldsymbol{U}_t+\boldsymbol{F}(\boldsymbol{U})_x+\boldsymbol{G}(\boldsymbol{U})_y=\boldsymbol{S}(\boldsymbol{U},B),\tag{2.21}$$

with $\boldsymbol{U}=(h,q^x,q^y)^\top$ and

$$\begin{aligned}&\boldsymbol{F}(\boldsymbol{U})=\left(q^x,\frac{(q^x)^2}{h}+\frac{g}{2}h^2,\frac{q^xq^y}{h}\right)^\top,\quad\boldsymbol{G}(\boldsymbol{U})=\left(q^y,\frac{q^xq^y}{h},\frac{(q^y)^2}{h}+\frac{g}{2}h^2\right)^\top,\\&\boldsymbol{S}(\boldsymbol{U},B)=(0,-ghB_x,-ghB_y)^\top.\end{aligned}\tag{2.22}$$

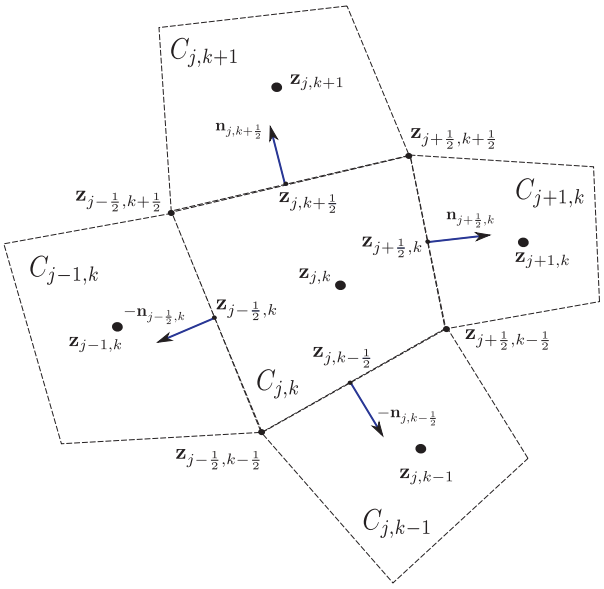

FIGURE 1. A typical quadrilateral cell $C_{j,k}$ with its four neighbors.

We apply the 2-D AMM central-upwind scheme from [19] to the system (2.21), (2.22). As in the 1-D case, we will need to develop the scheme that preserves the positivity of h and is well-balanced in the sense that it is capable of exactly preserving the "lake at rest" steady states ($w = \text{Const}$, $q^x \equiv q^y \equiv 0$).

Assume that the computational domain is covered with a structured irregular quadrilateral mesh consisting of cells $C_{j,k}$ of size $|C_{j,k}|$, and use the following notations (see Fig. 1):

$$\boldsymbol{z}_{j+\frac12,k+\frac12} := \Big(x_{j+\frac12,k+\frac12}, y_{j+\frac12,k+\frac12}\Big) : \text{ cell vertices},$$

$$\boldsymbol{z}_{j,k} := (x_{j,k}, y_{j,k}) : \text{ geometric center of } C_{j,k},$$

$$\ell_{j+\frac12,k} := \Big|\boldsymbol{z}_{j+\frac12,k+\frac12} - \boldsymbol{z}_{j+\frac12,k-\frac12}\Big| : \text{ length of the edge } \boldsymbol{z}_{j+\frac12,k-\frac12}\ \boldsymbol{z}_{j+\frac12,k+\frac12},$$

$$\boldsymbol{z}_{j+\frac12,k} := \frac12\Big(\boldsymbol{z}_{j+\frac12,k+\frac12} + \boldsymbol{z}_{j+\frac12,k-\frac12}\Big) : \text{ midpoint of the edge } \boldsymbol{z}_{j+\frac12,k-\frac12}\ \boldsymbol{z}_{j+\frac12,k+\frac12},$$

$$\boldsymbol{n}_{j+\frac12,k} := \Big(\cos\Big(\theta_{j+\frac12,k}\Big), \sin\Big(\theta_{j+\frac12,k}\Big)\Big) : \text{ the unit outer normal vector to the edge } \boldsymbol{z}_{j+\frac12,k-\frac12}\ \boldsymbol{z}_{j+\frac12,k+\frac12},$$

$$\ell_{j,k+\frac12} := \Big|\boldsymbol{z}_{j+\frac12,k+\frac12} - \boldsymbol{z}_{j-\frac12,k+\frac12}\Big| : \text{ length of the edge } \boldsymbol{z}_{j-\frac12,k+\frac12}\ \boldsymbol{z}_{j+\frac12,k+\frac12},$$

$$\boldsymbol{z}_{j,k+\frac12} := \frac12\Big(\boldsymbol{z}_{j+\frac12,k+\frac12} + \boldsymbol{z}_{j-\frac12,k+\frac12}\Big) : \text{ midpoint of the edge } \boldsymbol{z}_{j-\frac12,k+\frac12}\ \boldsymbol{z}_{j-\frac12,k+\frac12},$$

$$\boldsymbol{n}_{j,k+\frac12} := \Big(\cos\Big(\theta_{j,k+\frac12}\Big), \sin\Big(\theta_{j,k+\frac12}\Big)\Big) : \text{ the unit outer normal vector to the edge } \boldsymbol{z}_{j-\frac12,k+\frac12}\ \boldsymbol{z}_{j-\frac12,k+\frac12}.$$

Assume that at a certain time t, we have computed an approximate solution, realized in terms of its cell averages:

$$\overline{\boldsymbol{U}}_{j,k} \approx \frac{1}{|C_{j,k}|}\iint_{C_{j,k}} \boldsymbol{U}(x,y,t)\,\mathrm{d}x\,\mathrm{d}y.$$

They are then evolved from time level t to $t+\Delta t$ using the semi-discrete central-upwind scheme on structured quadrilateral grids from Section 2.2 of [19]:

$$\frac{\mathrm{d}}{\mathrm{d}t}\overline{\boldsymbol{U}}_{j,k}=-\frac{1}{|C_{j,k}|}\Big[\boldsymbol{H}_{j+\frac12,k}-\boldsymbol{H}_{j-\frac12,k}+\boldsymbol{H}_{j,k+\frac12}-\boldsymbol{H}_{j,k-\frac12}\Big]+\overline{\boldsymbol{S}}_{j,k}, \tag{2.23}$$

where the numerical fluxes along the boundaries of $C_{j,k}$ are given by

$$\boldsymbol{H}_{m,i}=\frac{\ell_{m,i}\Big(n^{(1)}_{m,i}\big[a^+_{m,i}\boldsymbol{F}^-_{m,i}-a^-_{m,i}\boldsymbol{F}^+_{m,i}\big]+n^{(2)}_{m,i}\big[a^+_{m,i}\boldsymbol{G}^-_{m,i}-a^-_{m,i}\boldsymbol{G}^+_{m,i}\big]+a^+_{m,i}a^-_{m,i}\big[\boldsymbol{U}^+_{m,i}-\boldsymbol{U}^-_{m,i}\big]\Big)}{a^+_{m,i}-a^-_{m,i}}, \tag{2.24}$$

and the second and third components of the cell averages of the source term $\overline{\boldsymbol{S}}_{j,k}$ are to be approximated in the well-balance manner; see Section 2.4.1.

In equation (2.24), $(m,i)=\big(j\pm\frac12,k\big)$ or $\big(j,k\pm\frac12\big)$, $\boldsymbol{F}^\pm_{m,i}:=\boldsymbol{F}\big(\boldsymbol{U}^\pm_{m,i}\big)$ and $\boldsymbol{G}^\pm_{m,i}:=\boldsymbol{G}\big(\boldsymbol{U}^\pm_{m,i}\big)$, where $\boldsymbol{U}^\pm_{m,i}$ are the reconstructed one-sided point values of $\boldsymbol{U}(\boldsymbol{z}_{m,i},t)$ computed along the normal to the corresponding cell edge (see Sect. 2.4.2), and $a^\pm_{m,i}$ are the directional local speeds of propagation (see Sect. 2.4.3).

2.4.1. Well-balanced source term quadratures

In order to derive the desired second-order well-balanced quadrature for the source term $\overline{S}^{(2)}_{j,k}$, we follow [3,7,21] and first use Green's formula together with the mean-value theorem to obtain

$$\begin{aligned}
\overline{S}^{(2)}_{j,k}&=-\frac{1}{|C_{j,k}|}\int_{C_{j,k}}ghB_x\,\mathrm{d}x\,\mathrm{d}y=-\frac{g}{|C_{j,k}|}\int_{C_{j,k}}(w-B)B_x\,\mathrm{d}x\,\mathrm{d}y\\
&=\frac{g}{|C_{j,k}|}\left[\int_{\partial C_{j,k}}\left(\frac{(w-B)^2}{2},0\right)\cdot\boldsymbol{n}\,\mathrm{d}s-\int_{C_{j,k}}(w-B)w_x\,\mathrm{d}x\,\mathrm{d}y\right]\\
&\approx\frac{g}{|C_{j,k}|}\left[\int_{\partial C_{j,k}}\left(\frac{h^2}{2},0\right)\cdot\boldsymbol{n}\,\mathrm{d}s-\overline{h}_{j,k}\int_{C_{j,k}}w_x\,\mathrm{d}x\,\mathrm{d}y\right]\\
&=\frac{g}{|C_{j,k}|}\left[\frac12\int_{\partial C_{j,k}}(h^2,0)\cdot\boldsymbol{n}\,\mathrm{d}s-\overline{h}_{j,k}\int_{\partial C_{j,k}}(w,0)\cdot\boldsymbol{n}\,\mathrm{d}s\right]=:\frac{g}{|C_{j,k}|}\Big[\mathrm{I}^{(2)}_{j,k}-\mathrm{II}^{(2)}_{j,k}\Big].
\end{aligned} \tag{2.25}$$

The line integrals in the terms $\mathrm{I}^{(2)}_{j,k}$ and $\mathrm{II}^{(2)}_{j,k}$ are then approximated using the midpoint rule, which results in

$$\mathrm{I}^{(2)}_{j,k}=\frac{\Big(h^-_{j+\frac12,k}\Big)^2\ell_{j+\frac12,k}n^{(1)}_{j+\frac12,k}-\Big(h^+_{j-\frac12,k}\Big)^2\ell_{j-\frac12,k}n^{(1)}_{j-\frac12,k}+\Big(h^-_{j,k+\frac12}\Big)^2\ell_{j,k+\frac12}n^{(1)}_{j,k+\frac12}-\Big(h^+_{j,k-\frac12}\Big)^2\ell_{j,k-\frac12}n^{(1)}_{j,k-\frac12}}{2}, \tag{2.26}$$

and

$$\mathrm{II}^{(2)}_{j,k}=\overline{h}_{j,k}\Big[w^-_{j+\frac12,k}\ell_{j+\frac12,k}n^{(1)}_{j+\frac12,k}-w^+_{j-\frac12,k}\ell_{j-\frac12,k}n^{(1)}_{j-\frac12,k}+w^-_{j,k+\frac12}\ell_{j,k+\frac12}n^{(1)}_{j,k+\frac12}-w^+_{j,k-\frac12}\ell_{j,k-\frac12}n^{(1)}_{j,k-\frac12}\Big]. \tag{2.27}$$

Finally, the cell average of the bottom topography,

$$\overline{B}_{j,k}\approx\frac{1}{|C_{j,k}|}\int_{C_{j,k}}B(x,y)\,\mathrm{d}x\,\mathrm{d}y, \tag{2.28}$$

should be numerically computed using a quadrature (in our numerical examples, we have split the quadrilateral $C_{j,k}$ into four triangles and used 7-point Gaussian quadrature in each of the triangles; see Appendix B for details).

Similarly, the well-balanced quadrature for $\overline{S}^{(3)}_{j,k}$ is

$$\overline{S}^{(3)}_{j,k}=\frac{g}{|C_{j,k}|}\Big[\mathrm{I}^{(3)}_{j,k}-\mathrm{II}^{(3)}_{j,k}\Big], \tag{2.29}$$

where

$$\mathrm{I}^{(3)}_{j,k}=\frac{\Big(h^-_{j+\frac12,k}\Big)^2\ell_{j+\frac12,k}n^{(2)}_{j+\frac12,k}-\Big(h^+_{j-\frac12,k}\Big)^2\ell_{j-\frac12,k}n^{(2)}_{j-\frac12,k}+\Big(h^-_{j,k+\frac12}\Big)^2\ell_{j,k+\frac12}n^{(2)}_{j,k+\frac12}-\Big(h^+_{j,k-\frac12}\Big)^2\ell_{j,k-\frac12}n^{(2)}_{j,k-\frac12}}{2}, \tag{2.30}$$

and

$$\mathrm{II}^{(3)}_{j,k}=\overline{h}_{j,k}\Big[w^-_{j+\frac12,k}\ell_{j+\frac12,k}n^{(2)}_{j+\frac12,k}-w^+_{j-\frac12,k}\ell_{j-\frac12,k}n^{(2)}_{j-\frac12,k}+w^-_{j,k+\frac12}\ell_{j,k+\frac12}n^{(2)}_{j,k+\frac12}-w^+_{j,k-\frac12}\ell_{j,k-\frac12}n^{(2)}_{j,k-\frac12}\Big]. \tag{2.31}$$

We now prove the well-balanced property of the resulting central-upwind scheme.

Theorem 2.7. *The central-upwind scheme* (2.23), (2.24) *with the numerical source terms given by* (2.25)–(2.31) *is well-balanced in the sense that it exactly preserves the "lake at rest" steady states*

$$\overline{w}_{j,k}\equiv\overline{w},\quad \bar{q}^x_{j,k}\equiv\bar{q}^y_{j,k}\equiv0. \tag{2.32}$$

Proof. Let us consider the second component of the scheme (2.23)–(2.31) and substitute (2.32) into it. The numerical fluxes are then equal to

$$H^{(2)}_{j+\frac12,k}=\frac{\Big(\overline{w}-B_{j+\frac12,k}\Big)^2}{2}\ell_{j+\frac12,k}n^{(1)}_{j+\frac12,k},\quad H^{(2)}_{j,k+\frac12}=\frac{\Big(\overline{w}-B_{j,k+\frac12}\Big)^2}{2}\ell_{j,k+\frac12}n^{(1)}_{j,k+\frac12},$$

which implies that

$$-\Big[H^{(2)}_{j+\frac12,k}-H^{(2)}_{j-\frac12,k}+H^{(2)}_{j,k+\frac12}-H^{(2)}_{j,k-\frac12}\Big]+g\mathrm{I}^{(2)}_{j,k}=0,\quad\forall j,k.$$

The second term in the numerical source is

$$\mathrm{II}^{(2)}_{j,k}=\big(\overline{w}-\overline{B}_{j,k}\big)\,\overline{w}\Big[\ell_{j+\frac12,k}n^{(1)}_{j+\frac12,k}-\ell_{j-\frac12,k}n^{(1)}_{j-\frac12,k}+\ell_{j,k+\frac12}n^{(1)}_{j,k+\frac12}-\ell_{j,k-\frac12}n^{(1)}_{j,k-\frac12}\Big],$$

and it is equal to zero since

$$\ell_{j+\frac12,k}n^{(1)}_{j+\frac12,k}-\ell_{j-\frac12,k}n^{(1)}_{j-\frac12,k}+\ell_{j,k+\frac12}n^{(1)}_{j,k+\frac12}-\ell_{j,k-\frac12}n^{(1)}_{j,k-\frac12}=\oint_{\partial C_{j,k}}(1,0)\cdot\boldsymbol{n}\,\mathrm{d}s=0.$$

Thus, we have proved that

$$\frac{\mathrm{d}}{\mathrm{d}t}\overline{U}^{(2)}_{j,k}=-\frac{1}{|C_{j,k}|}\Big[H^{(2)}_{j+\frac12,k}-H^{(2)}_{j-\frac12,k}+H^{(2)}_{j,k+\frac12}-H^{(2)}_{j,k-\frac12}\Big]+\frac{g}{|C_{j,k}|}\Big[\mathrm{I}^{(2)}_{j,k}-\mathrm{II}^{(2)}_{j,k}\Big]=0.$$

Similarly, one can show that

$$\frac{\mathrm{d}}{\mathrm{d}t}\overline{U}^{(3)}_{j,k}=0$$

at "lake at rest" steady states, which completes the proof of the theorem. □

2.4.2. Positivity preserving reconstruction

As in the 1-D case, we begin with applying the generalized minmod piecewise linear reconstruction, which has been extended to structured quadrilateral meshes in Section 2.2 of [19], to evaluate $w^{\pm}_{j+\frac12,k}$, $w^{\pm}_{j,k+\frac12}$, $(q^x)^{\pm}_{j+\frac12,k}$, $(q^x)^{\pm}_{j,k+\frac12}$, $(q^y)^{\pm}_{j+\frac12,k}$ and $(q^y)^{\pm}_{j,k+\frac12}$. In order to preserve the positivity of the water depth, we implement the same strategy as in the 1-D case and reconstruct h in the potentially dry areas.

Similarly to the 1-D case, the cell $C_{j,k}$ is called "dry" if the amount of water there is very small, namely, if at least one of the following inequalities is satisfied:

$$\min_{j',k':|j'-j|+|k'-k|\le1}\overline{w}_{j',k'} < \max_{(x,y)\in\Omega_{j,k}} B(x,y), \tag{2.33}$$

$$\overline{w}_{j,k}-\overline{B}_{j,k}<\delta, \tag{2.34}$$

where $\Omega_{j,k}:=\big\{(x,y)\in C_{j',k'}\big|\,|j'-j|+|k'-k|\le1\big\}$, $\delta>0$ is the same small parameter as in (2.7), and $\overline{B}_{j,k}$ is given by (2.28). All other cells are called "wet".

As in the 1-D case, in "dry" cells, we use the piecewise linear positivity preserving reconstruction (described in [19], Sect. 2.2) of h based on the cell averages of water depth $\overline{h}_{j,k}:=\overline{w}_{j,k}-\overline{B}_{j,k}$. After computing $h^-_{j+\frac12,k}$, $h^+_{j-\frac12,k}$, $h^-_{j,k+\frac12}$ and $h^+_{j,k-\frac12}$ in the "dry" cell $C_{j,k}$, we obtain $w^+_{j-\frac12,k}:=h^+_{j-\frac12,k}+B_{j-\frac12,k}$, $w^-_{j+\frac12,k}:=h^-_{j+\frac12,k}+B_{j+\frac12,k}$, $w^+_{j,k-\frac12}:=h^+_{j,k-\frac12}+B_{j,k-\frac12}$ and $w^-_{j,k+\frac12}:=h^-_{j,k+\frac12}+B_{j,k+\frac12}$ there.

Remark 2.8. In practice, one may replace the condition (2.33) with its simplified version:

$$\min_{|j'-j|+|k'-k|\le1}\overline{w}_{j',k'} < \max\Big\{\overline{B}_{j,k},\overline{B}_{j+1,k},\overline{B}_{j,k+1},\overline{B}_{j-1,k},\overline{B}_{j,k-1},B_{j+\frac12,k},B_{j-\frac12,k},B_{j,k+\frac12},B_{j,k-\frac12}\Big\}, \tag{2.35}$$

which is much easier to check. As in the 1-D casse, the use of the simplified condition (2.35) does not guarantee positivity of the projected values of h, but negative h may appear only in a small number of cells located near the wet/dry interfaces. If this occurs, we reclassify these particular cells from "wet" to "dry" and reconstruct h instead of w in them.

2.4.3. Desingularization and directional local speeds

Similarly to the 1-D case, we follow [18] and desingularize the computation of the velocity point values needed to evaluate numerical fluxes by setting

$$u^{\pm}_{m,i}=\frac{\sqrt{2}\,h^{\pm}_{m,i}\,(q^x)^{\pm}_{m,i}}{\sqrt{\big(h^{\pm}_{m,i}\big)^4+\max\Big[\big(h^{\pm}_{m,i}\big)^4,\varepsilon^4\Big]}},\quad v^{\pm}_{m,i}=\frac{\sqrt{2}\,h^{\pm}_{m,i}\,(q^y)^{\pm}_{m,i}}{\sqrt{\big(h^{\pm}_{m,i}\big)^4+\max\Big[\big(h^{\pm}_{m,i}\big)^4,\varepsilon^4\Big]}} \tag{2.36}$$

where $(m,i)=\big(j+\frac12,k\big)$ or $\big(j,k+\frac12\big)$ and then for consistency we modify the corresponding values of the discharges by recalculating

$$(q^x)^{\pm}_{m,i}=h^{\pm}_{m,i}\cdot u^{\pm}_{m,i},\quad (q^y)^{\pm}_{m,i}=h^{\pm}_{m,i}\cdot v^{\pm}_{m,i}.$$

In (2.36), ε is a small desingularization parameter, which we take to be equal to δ in (2.34).

Equipped with the values $h^{\pm}_{m,i}$, $u^{\pm}_{m,i}$, and $v^{\pm}_{m,i}$, we estimate the directional local speeds of propagation needed in (2.24) as follows:

$$a^+_{m,i}=\max\Big\{\mathcal{V}^{\pm}_{m,i}+\sqrt{gh^{\pm}_{m,i}},\,0\Big\},\quad a^-_{m,i}=\min\Big\{\mathcal{V}^{\pm}_{m,i}-\sqrt{gh^{\pm}_{m,i}},\,0\Big\},$$

where $\mathcal{V}$ is the velocity in the direction normal to the corresponding side of $C_{j,k}$, namely,

$$\mathcal{V}^{\pm}_{m,i}:=\boldsymbol{n}_{m,i}\cdot\big(u^{\pm}_{m,i},v^{\pm}_{m,i}\big). \tag{2.37}$$

2.4.4. Positivity preserving evolution

As in the 1-D case, we enforce the positivity of h during the evolution step by implementing the draining time-step technique from [4].

We first consider the forward Euler discretization of (2.23), the first component of which reads as

$$\overline{h}_{j,k}(t+\Delta t)=\overline{h}_{j,k}(t)-\frac{\Delta t}{|C_{j,k}|}\Big[H^{(1)}_{j+\frac12,k}-H^{(1)}_{j-\frac12,k}+H^{(1)}_{j,k+\frac12}-H^{(1)}_{j,k-\frac12}\Big], \tag{2.38}$$

where Δt is the time step constrained by the CFL condition:

$$\Delta t\max_{j,k}\{\Psi_{j,k}\}\le 1,\quad \Psi_{j,k}:=\frac{\max\Big\{\Big|a^-_{j+\frac12,k}\Big|,\Big|a^+_{j-\frac12,k}\Big|,\Big|a^-_{j,k+\frac12}\Big|,\Big|a^+_{j,k-\frac12}\Big|\Big\}}{\operatorname{dist}(\boldsymbol{z}_{j,k},\partial C_{j,k})}.$$

We then denote by

$$\Delta t^{\rm drain}_{j,k}:=\frac{|C_{j,k}|\,\overline{h}_{j,k}(t)}{\max\Big(0,H^{(1)}_{j+\frac12,k}\Big)+\max\Big(0,-H^{(1)}_{j-\frac12,k}\Big)+\max\Big(0,H^{(1)}_{j,k+\frac12}\Big)+\max\Big(0,-H^{(1)}_{j,k+\frac12}\Big)},$$

and replace (2.38) with

$$\overline{h}_{j,k}(t+\Delta t)=\overline{h}_{j,k}(t)-\frac{1}{|C_{j,k}|}\Big[\Delta t_{j+\frac12,k}H^{(1)}_{j+\frac12,k}-\Delta t_{j-\frac12,k}H^{(1)}_{j-\frac12,k}+\Delta t_{j,k+\frac12}H^{(1)}_{j,k+\frac12}-\Delta t_{j,k-\frac12}H^{(1)}_{j,k-\frac12}\Big],$$

where $\Delta t_{j+\frac12,k}$ and $\Delta t_{j,k+\frac12}$ are defined as follows:

$$\Delta t_{j+\frac12,k}=\min\big(\Delta t,\Delta t^{\rm drain}_{i,k}\big),\quad i=j+\frac12-\frac{\operatorname{sgn}\Big(H^{(1)}_{j+\frac12,k}\Big)}{2},$$
$$\Delta t_{j,k+\frac12}=\min\big(\Delta t,\Delta t^{\rm drain}_{j,i}\big),\quad i=k+\frac12-\frac{\operatorname{sgn}\Big(H^{(1)}_{j,k+\frac12}\Big)}{2}.$$

The corresponding forward Euler steps for q^x and q^y are

$$\begin{aligned}\overline{q^x}_{j,k}(t+\Delta t)=\overline{q^x}_{j,k}(t)&-\frac{1}{|C_{j,k}|}\Big[\Delta t_{j+\frac12,k}H^{(a,2)}_{j+\frac12,k}-\Delta t_{j-\frac12,k}H^{(a,2)}_{j-\frac12,k}+\Delta t_{j,k+\frac12}H^{(a,2)}_{j,k+\frac12}-\Delta t_{j,k-\frac12}H^{(a,2)}_{j,k-\frac12}\Big]\\&-\frac{\Delta t}{|C_{j,k}|}\Big[H^{(g,2)}_{j+\frac12,k}-H^{(g,2)}_{j-\frac12,k}+H^{(g,2)}_{j,k+\frac12}-H^{(g,2)}_{j,k-\frac12}\Big]+\Delta t\,\overline{S}^{(2)}_{j,k},\\
\overline{q^y}_{j,k}(t+\Delta t)=\overline{q^y}_{j,k}(t)&-\frac{1}{|C_{j,k}|}\Big[\Delta t_{j+\frac12,k}H^{(a,3)}_{j+\frac12,k}-\Delta t_{j-\frac12,k}H^{(a,3)}_{j-\frac12,k}+\Delta t_{j,k+\frac12}H^{(a,3)}_{j,k+\frac12}-\Delta t_{j,k-\frac12}H^{(a,3)}_{j,k-\frac12}\Big]\\&-\frac{\Delta t}{|C_{j,k}|}\Big[H^{(g,3)}_{j+\frac12,k}-H^{(g,3)}_{j-\frac12,k}+H^{(g,3)}_{j,k+\frac12}-H^{(g,3)}_{j,k-\frac12}\Big]+\Delta t\,\overline{S}^{(3)}_{j,k},\end{aligned}$$

where the advective and gravitational parts of the fluxes can be obtained by

$$
\begin{aligned}
H^{(a,2)}_{m,i} &= \frac{\ell_{m,i}}{a^+_{m,i}-a^-_{m,i}}\Big\{n^{(1)}_{m,i}\Big[a^+_{m,i}h^-_{m,i}\big(u^-_{m,i}\big)^2-a^-_{m,i}h^+_{m,i}\big(u^+_{m,i}\big)^2\Big]\\
&\quad+n^{(2)}_{m,i}\big[a^+_{m,i}h^-_{m,i}u^-_{m,i}v^-_{m,i}-a^-_{m,i}h^+_{m,i}u^+_{m,i}v^+_{m,i}\big]\Big\},\\
H^{(g,2)}_{m,i} &= \frac{\ell_{m,i}}{a^+_{m,i}-a^-_{m,i}}\left\{\frac{gn^{(1)}_{m,i}}{2}\Big[a^+_{m,i}\big(h^-_{m,i}\big)^2-a^-_{m,i}\big(h^+_{m,i}\big)^2\Big]+a^+_{m,i}a^-_{m,i}\big[(q^x)^+_{m,i}-(q^x)^-_{m,i}\big]\right\},\\
H^{(a,3)}_{m,i} &= \frac{\ell_{m,i}}{a^+_{m,i}-a^-_{m,i}}\Big\{n^{(1)}_{m,i}\big[a^+_{m,i}h^-_{m,i}u^-_{m,i}v^-_{m,i}-a^-_{m,i}h^+_{m,i}u^+_{m,i}v^+_{m,i}\big]\\
&\quad+n^{(2)}_{m,i}\Big[a^+_{m,i}h^-_{m,i}\big(v^-_{m,i}\big)^2-a^-_{m,i}h^+_{m,i}\big(v^+_{m,i}\big)^2\Big]\Big\},\\
H^{(g,3)}_{m,i} &= \frac{\ell_{m,i}}{a^+_{m,i}-a^-_{m,i}}\left\{\frac{gn^{(2)}_{m,i}}{2}\Big[a^+_{m,i}\big(h^-_{m,i}\big)^2-a^-_{m,i}\big(h^+_{m,i}\big)^2\Big]+a^+_{m,i}a^-_{m,i}\big[(q^y)^+_{m,i}-(q^y)^-_{m,i}\big]\right\},
\end{aligned}
$$

with $(m,i)=\big(j+\frac12,k\big)$ or $\big(j,k+\frac12\big)$.

Remark 2.9. Similarly to the 1-D case, one can alternatively use a more restrictive CFL condition (derived in Appendix C.2) to ensure the positivity of h during the time evolution, but this will slow down the computations by a factor of about 2. At the same time, as in the 1-D case the use of smaller CFL number does not lead to any improvement in the quality of the computed solutions. In all of the numerical examples reported in Section 3, we have used the draining time-step technique.

2.5. Two-dimensional moving mesh equation

In this section, we briefly describe the 2-D MMPDE and its numerical solution algorithm; see Section 3.2 of [19] for details.

Assume that the computational domain $[a,b]\times[c,d]$ is covered by the nonuniform mesh $\Big\{x_{j+\frac12,k+\frac12},y_{j+\frac12,k+\frac12}\Big\}$. We introduce the uniform rectangular logical mesh

$$
\Big\{(\xi_{j+\frac12},\eta_{k+\frac12})\;\Big|\;\xi_{j+\frac12}=j\Delta\xi,\;\eta_{k+\frac12}=k\Delta\eta\Big\},\quad j=0,\ldots,N,\quad k=0,\ldots,M,
$$

where $\Delta\xi=1/N$ and $\Delta\eta=1/M$ are the spatial scales in the ξ- and η-directions, respectively. Let us denote the one-to-one coordinate transformation from the logical domain to the computational one by

$$
(x,y)=(x(\xi,\eta),y(\xi,\eta)),\quad (\xi,\eta)\in[0,1]\times[0,1],
$$

so that $x_{j+\frac12,k+\frac12}=x(\xi_{j+\frac12},\eta_{k+\frac12})$ and $y_{j+\frac12,k+\frac12}=y(\xi_{j+\frac12},\eta_{k+\frac12})$. We assume that $x(0,\eta)=a$ and $x(1,\eta)=b$ for all η as well as $y(\xi,0)=c$ and $y(\xi,1)=d$ for all ξ.

The mesh is distributed according to the following MMPDE:

$$
(\omega\boldsymbol{z}_\xi)_\xi+(\omega\boldsymbol{z}_\eta)_\eta=\boldsymbol{0},\quad \omega(\boldsymbol{U})=1+\alpha\varphi(\|D\boldsymbol{U}\|),\tag{2.39}
$$

where $\boldsymbol{z}:=(x,y)$, ω is a monitor function, and D is a differential operator. In this paper, we use $D\boldsymbol{U}=U^{(i)}_{\xi\xi}+U^{(i)}_{\eta\eta}$ (for some component of $\boldsymbol{U}$), which is approximated using the second-order centered differences:

$$
D\boldsymbol{U}_{j,k}=\Big(U^{(i)}_{\xi\xi}\Big)_{j,k}+\Big(U^{(i)}_{\eta\eta}\Big)_{j,k}=\frac{\overline{U}^{(i)}_{j+1,k}-2\overline{U}^{(i)}_{j,k}+\overline{U}^{(i)}_{j-1,k}}{(\Delta\xi)^2}+\frac{\overline{U}^{(i)}_{j,k+1}-2\overline{U}^{(i)}_{j,k}+\overline{U}^{(i)}_{j,k-1}}{(\Delta\eta)^2}.
$$

The function φ in (2.39) is a smoothing filter designed as follows. We first compute $\varphi^0_{j,k} := |D\boldsymbol{U}_{j,k}|$ and then smooth $\varphi^0_{j,k}$ out by averaging the values over the neighboring cells for each j,k for a prescribed number of iterations, that is, we introduce

$$\varphi^{\ell+1}_{j,k} = \frac{1}{4}\,\varphi^{\ell}_{j,k} + \frac{1}{8}\big(\varphi^{\ell}_{j,k-1} + \varphi^{\ell}_{j,k+1} + \varphi^{\ell}_{j-1,k} + \varphi^{\ell}_{j+1,k}\big) + \frac{1}{16}\big(\varphi^{\ell}_{j-1,k-1} + \varphi^{\ell}_{j+1,k-1} + \varphi^{\ell}_{j-1,k+1} + \varphi^{\ell}_{j+1,k+1}\big), \quad \ell = 0,\dots,m-1,$$

and then set $\big(\varphi(\|D\boldsymbol{U}\|)\big)_{j,k} := \varphi^m_{j,k}$, which is used in (2.39). In our numerical experiments, we have taken $m = 4$.

Finally, α in (2.39) is an intensity parameter needed to control the mesh concentration. In our computation, we choose α to be

$$\alpha = \left(\frac{1-\beta}{\beta(b-a)(d-c)}\iint_{[a,b]\times[c,d]}\varphi(\|D\boldsymbol{U}\|)\,\mathrm{d}x\,\mathrm{d}y\right)^{-1},$$

where $\beta \in (0,1)$ is the prescribed fraction of mesh points to be concentrated at the "rough" areas of the computed solution.

Equipped with the monitor function ω, we discretize the MMPDEs (2.39) using the centered difference approximation, which results in the following linear algebraic system for the mesh points locations:

$$\begin{cases} x_{\frac12,k+\frac12} = a, \quad x_{N+\frac12,k+\frac12} = b, & k = 0,\dots,M\\ \dfrac{\omega_{j+1,k+\frac12}\Big(x_{j+\frac32,k+\frac12} - x_{j+\frac12,k+\frac12}\Big) - \omega_{j,k+\frac12}\Big(x_{j+\frac12,k+\frac12} - x_{j-\frac12,k+\frac12}\Big)}{(\Delta\xi)^2}\\ \quad + \dfrac{\omega_{j+\frac12,k+1}\Big(x_{j+\frac12,k+\frac32} - x_{j+\frac12,k+\frac12}\Big) - \omega_{j+\frac12,k}\Big(x_{j+\frac12,k+\frac12} - x_{j+\frac12,k-\frac12}\Big)}{(\Delta\eta)^2} = 0, & 1\le j\le N-1,\ 0\le k\le M,\\ x_{j+\frac12,-\frac12} = x_{j+\frac12,\frac32}, \quad x_{j+\frac12,M+\frac32} = x_{j+\frac12,M-\frac12}, & j = 0,\dots,N, \end{cases}$$

$$\begin{cases} y_{j+\frac12,\frac12} = c, \quad y_{j+\frac12,M+\frac12} = d, & j = 0,\dots,N\\ \dfrac{\omega_{j+1,k+\frac12}\Big(y_{j+\frac32,k+\frac12} - y_{j+\frac12,k+\frac12}\Big) - \omega_{j,k+\frac12}\Big(y_{j+\frac12,k+\frac12} - y_{j-\frac12,k+\frac12}\Big)}{(\Delta\xi)^2}\\ \quad + \dfrac{\omega_{j+\frac12,k+1}\Big(y_{j+\frac12,k+\frac32} - y_{j+\frac12,k+\frac12}\Big) - \omega_{j+\frac12,k}\Big(y_{j+\frac12,k+\frac12} - y_{j+\frac12,k-\frac12}\Big)}{(\Delta\eta)^2} = 0, & 0\le j\le N,\ 1\le k\le M-1,\\ y_{-\frac12,k+\frac12} = y_{\frac32,k+\frac12}, \quad y_{N+\frac32,k+\frac12} = y_{N-\frac12,k+\frac12}, & k = 0,\dots,M, \end{cases}$$

where $\omega_{j,k+\frac12} := (\omega_{j,k} + \omega_{j,k+1})/2$ and $\omega_{j+\frac12,k} := (\omega_{j,k} + \omega_{j+1,k})/2$. Similarly to the 1-D case, we numerically solve this system using the Jacobi iterations combined with the mesh relaxation procedure to avoid rapid change of mesh. Denoting by $\boldsymbol{z}^{\nu}_{j+\frac12,k+\frac12}$ the grid nodes in the beginning of the $(\nu+1)$th iteration step (with the initial guess $\boldsymbol{z}^{0}_{j+\frac12,k+\frac12}$ being the grid nodes from the previous evolution step), we take one Jacobi sweep

$$x^*_{j+\frac12,k+\frac12} = \frac{\Big(\omega^{\nu}_{j+\frac12,k+1}x^{\nu}_{j+\frac12,k+\frac32} + \omega^{\nu}_{j+\frac12,k}x^{\nu}_{j+\frac12,k-\frac12}\Big)\Delta\xi^2 + \Big(\omega^{\nu}_{j+1,k+\frac12}x^{\nu}_{j+\frac32,k+\frac12} + \omega^{\nu}_{j,k+\frac12}x^{\nu}_{j-\frac12,k+\frac12}\Big)\Delta\eta^2}{\Big(\omega^{\nu}_{j+\frac12,k+1} + \omega^{\nu}_{j+\frac12,k}\Big)\Delta\xi^2 + \Big(\omega^{\nu}_{j+1,k+\frac12} + \omega^{\nu}_{j,k+\frac12}\Big)\Delta\eta^2}, \quad 1\le j\le N-1, \quad 0\le k\le M,$$

$$y^*_{j+\frac12,k+\frac12} = \frac{\Big(\omega^{\nu}_{j+\frac12,k+1}y^{\nu}_{j+\frac12,k+\frac32} + \omega^{\nu}_{j+\frac12,k}y^{\nu}_{j+\frac12,k-\frac12}\Big)\Delta\xi^2 + \Big(\omega^{\nu}_{j+1,k+\frac12}y^{\nu}_{j+\frac32,k+\frac12} + \omega^{\nu}_{j,k+\frac12}y^{\nu}_{j-\frac12,k+\frac12}\Big)\Delta\eta^2}{\Big(\omega^{\nu}_{j+\frac12,k+1} + \omega^{\nu}_{j+\frac12,k}\Big)\Delta\xi^2 + \Big(\omega^{\nu}_{j+1,k+\frac12} + \omega^{\nu}_{j,k+\frac12}\Big)\Delta\eta^2}, \quad 0\le j\le N, \quad 1\le k\le M-1,$$

where $\omega^{\nu}_{j,k+\frac12}$ and $\omega^{\nu}_{j+\frac12,k}$ are the values of the monitor function ω at the grid points $\boldsymbol{z}=\boldsymbol{z}^{\nu}_{j,k+\frac12}$ and $\boldsymbol{z}=\boldsymbol{z}^{\nu}_{j+\frac12,k}$, respectively, computed using the cell averages $\left\{\overline{\boldsymbol{U}}^{\nu}_{j,k}\right\}$. This results in the grid $\left\{\boldsymbol{z}^{*}_{j+\frac12,k+\frac12}\right\}=\left\{\left(x^{*}_{j+\frac12,k+\frac12},y^{*}_{j+\frac12,k+\frac12}\right)\right\}$, which is then relaxed by setting

$$\boldsymbol{z}^{\nu+1}_{j+\frac12,k+\frac12}=\frac12\left(\boldsymbol{z}^{\nu}_{j+\frac12,k+\frac12}+\boldsymbol{z}^{*}_{j+\frac12,k+\frac12}\right),\quad j=1,\ldots,N-1,\quad k=1,\ldots,M-1. \tag{2.40}$$

Remark 2.10. Similarly to 1-D case, we stop the iteration process in (2.40) after a fixed number of iterations. In all of our numerical experiments, the upper bound on the number of iterations has been set to 4.

2.6. Two-dimensional conservative positivity preserving projection

After obtaining the new mesh, we need to project the solution from the cells $C^{\nu}_{j,k}$, whose vertices are $\boldsymbol{z}^{\nu}_{j\pm\frac12,k\pm\frac12}$, to the new cells $C^{\nu+1}_{j,k}$ with the vertices $\boldsymbol{z}^{\nu+1}_{j\pm\frac12,k\pm\frac12}$.

We denote by $\overline{\boldsymbol{U}}^{\nu}_{j,k}$ and $\overline{\boldsymbol{U}}^{\nu+1}_{j,k}$ the cell averages over the cells $C^{\nu}_{j,k}$ and $C^{\nu+1}_{j,k}$, respectively, and introduce the following quantities measuring the mesh shift (for their precise geometric meaning; see [19], Sect. 3.2):

$$\mu^{\nu+\frac12}_{j+\frac12,k}=\frac12\left[\left(x^{\nu+1}_{j+\frac12,k-\frac12}-x^{\nu}_{j+\frac12,k+\frac12}\right)\left(y^{\nu+1}_{j+\frac12,k+\frac12}-y^{\nu}_{j+\frac12,k-\frac12}\right)-\left(x^{\nu+1}_{j+\frac12,k+\frac12}-x^{\nu}_{j+\frac12,k-\frac12}\right)\left(y^{\nu+1}_{j+\frac12,k-\frac12}-y^{\nu}_{j+\frac12,k+\frac12}\right)\right],$$
$$\mu^{\nu+\frac12}_{j,k+\frac12}=\frac12\left[\left(x^{\nu+1}_{j+\frac12,k+\frac12}-x^{\nu}_{j-\frac12,k+\frac12}\right)\left(y^{\nu+1}_{j-\frac12,k+\frac12}-y^{\nu}_{j+\frac12,k+\frac12}\right)-\left(x^{\nu+1}_{j-\frac12,k+\frac12}-x^{\nu}_{j+\frac12,k+\frac12}\right)\left(y^{\nu+1}_{j+\frac12,k+\frac12}-y^{\nu}_{j-\frac12,k+\frac12}\right)\right].$$

The conservative solution projection step from [22] is given by

$$\left|C^{\nu+1}_{j,k}\right|\overline{\boldsymbol{U}}^{\nu+1}_{j,k}=\left|C^{\nu}_{j,k}\right|\overline{\boldsymbol{U}}^{\nu}_{j,k}+\mu^{\nu+\frac12}_{j+\frac12,k}\boldsymbol{U}^{\nu}_{j+\frac12,k}-\mu^{\nu+\frac12}_{j-\frac12,k}\boldsymbol{U}^{\nu}_{j-\frac12,k}+\mu^{\nu+\frac12}_{j,k+\frac12}\boldsymbol{U}^{\nu}_{j,k+\frac12}-\mu^{\nu+\frac12}_{j,k-\frac12}\boldsymbol{U}^{\nu}_{j,k-\frac12},$$

where

$$\boldsymbol{U}^{\nu}_{j+\frac12,k}:=\begin{cases}\boldsymbol{U}^{+}_{j+\frac12,k},&\text{if }\ \mu^{\nu+\frac12}_{j+\frac12,k}>0,\\ \boldsymbol{U}^{-}_{j+\frac12,k},&\text{if }\ \mu^{\nu+\frac12}_{j+\frac12,k}<0,\end{cases}\qquad \boldsymbol{U}^{\nu}_{j,k+\frac12}:=\begin{cases}\boldsymbol{U}^{+}_{j,k+\frac12},&\text{if }\ \mu^{\nu+\frac12}_{j,k+\frac12}>0,\\ \boldsymbol{U}^{-}_{j,k+\frac12},&\text{if }\ \mu^{\nu+\frac12}_{j,k+\frac12}<0,\end{cases} \tag{2.41}$$

and $\boldsymbol{U}^{\pm}_{j+\frac12,k}$ and $\boldsymbol{U}^{\pm}_{j,k+\frac12}$ are the point values reconstructed over the grid $C^{\nu}_{j,k}$ as described in Section 2.4.2.

In particular, this projection step for the water surface variable w reads as

$$\left|C^{\nu+1}_{j,k}\right|\overline{w}^{\nu+1}_{j,k}=\left|C^{\nu}_{j,k}\right|\overline{w}^{\nu}_{j,k}+\mu^{\nu+\frac12}_{j+\frac12,k}w^{\nu}_{j+\frac12,k}-\mu^{\nu+\frac12}_{j-\frac12,k}w^{\nu}_{j-\frac12,k}+\mu^{\nu+\frac12}_{j,k+\frac12}w^{\nu}_{j,k+\frac12}-\mu^{\nu+\frac12}_{j,k-\frac12}w^{\nu}_{j,k-\frac12}. \tag{2.42}$$

Again, by the same reason as in the 1-D case, this projection step cannot be used in the "dry" areas, and therefore we replace the projection step (2.42) with

$$\left|C^{\nu+1}_{j,k}\right|\overline{w}^{\nu+1}_{j,k}=\left|C^{\nu}_{j,k}\right|\overline{w}^{\nu}_{j,k}+\mu^{\nu+\frac12}_{j+\frac12,k}\widetilde{w}^{\nu}_{j+\frac12,k}-\mu^{\nu+\frac12}_{j-\frac12,k}\widetilde{w}^{\nu}_{j-\frac12,k}+\mu^{\nu+\frac12}_{j,k+\frac12}\widetilde{w}^{\nu}_{j,k+\frac12}-\mu^{\nu+\frac12}_{j,k-\frac12}\widetilde{w}^{\nu}_{j,k-\frac12}+B^{\mathrm{corr}}_{j,k},$$

where

$$\widetilde{w}^{\nu}_{j+\frac12,k}:=\begin{cases}w^{\nu}_{j+\frac12,k},&\text{if } C_{j,k}\text{ is ``wet'' and }\mu^{\nu+\frac12}_{j+\frac12,k}\le0\text{ or }C_{j+1,k}\text{ is ``wet'' and }\mu^{\nu+\frac12}_{j+\frac12,k}\ge0,\\ h^{\nu}_{j+\frac12,k}+\overline{B}^{\nu+\frac12}_{j+\frac12,k},&\text{otherwise,}\end{cases}$$

and

$$\widetilde{w}^{\nu}_{j,k+\frac12}:=\begin{cases}w^{\nu}_{j,k+\frac12},&\text{if } C_{j,k}\text{ is ``wet'' and }\mu^{\nu+\frac12}_{j,k+\frac12}\le0\text{ or }C_{j,k+1}\text{ is ``wet'' and }\mu^{\nu+\frac12}_{j,k+\frac12}\ge0,\\ h^{\nu}_{j,k+\frac12}+\overline{B}^{\nu+\frac12}_{j,k+\frac12},&\text{otherwise.}\end{cases}$$

Here, $w^{\nu}_{j+\frac12,k}$, $w^{\nu}_{j,k+\frac12}$, $h^{\nu}_{j+\frac12,k}$ and $h^{\nu}_{j,k+\frac12}$ are determined using (2.41), and

$$\overline{B}^{\nu+\frac12}_{j+\frac12,k}\approx\frac{1}{\mu^{\nu+\frac12}_{j+\frac12,k}}\int_{C^{\nu}_{j+\frac12,k}}B(x,y)\,\mathrm{d}x\,\mathrm{d}y,\quad C^{\nu+\frac12}_{j+\frac12,k}:=\boldsymbol{z}^{\nu}_{j+\frac12,k+\frac12}\boldsymbol{z}^{\nu}_{j+\frac12,k-\frac12}\boldsymbol{z}^{\nu+1}_{j+\frac12,k-\frac12}\boldsymbol{z}^{\nu+1}_{j+\frac12,k+\frac12},\tag{2.43}$$

and

$$\overline{B}^{\nu+\frac12}_{j,k+\frac12}\approx\frac{1}{\mu^{\nu+\frac12}_{j,k+\frac12}}\int_{C^{\nu}_{j,k+\frac12}}B(x,y)\,\mathrm{d}x\,\mathrm{d}y,\quad C^{\nu+\frac12}_{j,k+\frac12}:=\boldsymbol{z}^{\nu}_{j-\frac12,k+\frac12}\boldsymbol{z}^{\nu}_{j+\frac12,k+\frac12}\boldsymbol{z}^{\nu+1}_{j+\frac12,k+\frac12}\boldsymbol{z}^{\nu+1}_{j-\frac12,k+\frac12},\tag{2.44}$$

are approximations of the averages of B over the quadrilaterals $C^{\nu+\frac12}_{j+\frac12,k}$ and $C^{\nu+\frac12}_{j,k+\frac12}$, respectively. In our numerical examples, we have evaluated the integrals in (2.43) and (2.44) by splitting the quadrilaterals $C^{\nu+\frac12}_{j+\frac12,k}$ and $C^{\nu+\frac12}_{j,k+\frac12}$ into the four corresponding triangles and then using in each of the triangles the 7-point Gaussian quadrature, described in Appendix B. Finally, the "dry" cell correction term $B^{\rm corr}_{j,k}$ is defined as

$$B^{\rm corr}_{j,k}:=\begin{cases}0, & \text{if } C_{j,k} \text{ is ``wet''},\\ \left|C^{\nu+1}_{j,k}\right|\overline{B}^{\nu+1}_{j,k}-\Big[\left|C^{\nu}_{j,k}\right|\overline{B}^{\nu}_{j,k}+\mu^{\nu+\frac12}_{j+\frac12,k}\overline{B}^{\nu+\frac12}_{j+\frac12,k}-\mu^{\nu+\frac12}_{j-\frac12,k}\overline{B}^{\nu+\frac12}_{j-\frac12,k}\\ \qquad\qquad+\mu^{\nu+\frac12}_{j,k+\frac12}\overline{B}^{\nu+\frac12}_{j,k+\frac12}-\mu^{\nu+\frac12}_{j,k-\frac12}\overline{B}^{\nu+\frac12}_{j,k-\frac12}\Big], & \text{otherwise.}\end{cases}$$

Remark 2.11. For long time simulations, the mesh grid distribution may not be balanced around the shocks, and as a result, more grid points can be concentrated on one side of the shock curve than on the other side. This can be fixed by increasing the number of iterations of moving mesh process, since within 1–4 iterations only few grid points can cross the shock curve. In this case, however, the resulting method will be extremely inefficient. In order to improve the efficiency of the AMM algorithm, we re-project the solution back onto uniform mesh from time to time and then re-start the moving mesh adjustment. This significantly improves the distribution of resulting meshes. In all of our numerical experiments, we re-project the solution based on its second-order reconstruction.

3. Numerical examples

In this section, we test the developed AMM central-upwind schemes for the 1-D and 2-D Saint-Venant systems and compare the obtained results with the ones computed by the central-upwind scheme from [18] implemented on uniform meshes.

In all of the examples, the minmod parameter in the piecewise linear reconstructions is taken to be 1.3; see [19] for details.

The ODE systems (2.3) and (2.23) are numerically solved by the three-stage third-order SSP Runge–Kutta method. Each forward Euler stage of the SSP solver is described in Sections 2.1.3 and 2.4.4 for the 1-D and 2-D case, respectively.

Remark 3.1. The parameter β will be taken different in different examples as the fraction of mesh points that needs to be concentrated in the "rough" areas of the solution depends on the structure of the solution, in particular, on the numbers and distribution of shocks. One can also select β dynamically in order to keep the smallest cell and/or time step sizes within a tolerable range. This is, however, beyond the scope of the current paper.

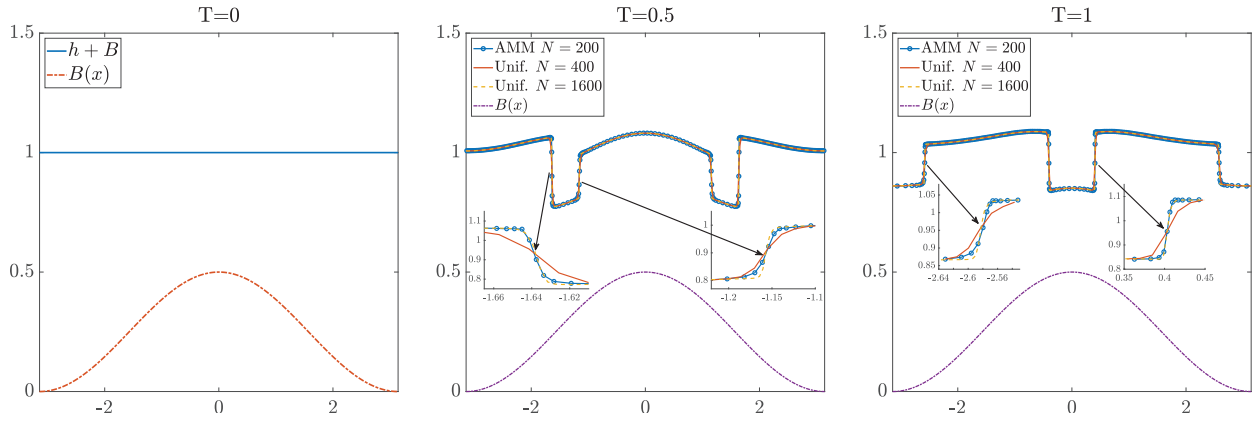

FIGURE 2. Example 1: Initial condition and solution profiles (w and B) computed by the AAM and uniform grid central-upwind schemes at different times.

Example 1 – One-dimensional case

In this example, we solve the 1-D Saint-Venant system of shallow water equations on the computational domain $[-\pi,\pi]$ with the bottom topography consisting of one hump,

$$B(x)=\frac{1}{4}(1+\cos x),$$

the following initial conditions:

$$w(x,0)\equiv 1,\quad u(x,0)=-\text{sign}(x)\cos x.$$

and the (reflective) solid wall boundary conditions at both $x=\pm\pi$.

We initially split the computational domain into $N=200$ uniform finite-volume cells and compute the solution by the proposed AMM central-upwind scheme using the monitor function in (2.11) with $D\boldsymbol{U}=w_{\xi\xi}$ and the mesh concentration parameter $\beta=0.8$.

In Figure 2, we plot the water surface w together with the bottom topography B at times $t=0$, 0.5 and 2. As one can see, the AMM results are sharper than the ones obtained using the uniform mesh with $N=400$ and are comparible with the ones computed using the uniform mesh with $N=1600$. In Figure 3 (left), we present the corresponding time-space distribution of mesh cells, which clearly shows that the AMM is able to capture and follow the solution discontinuities. Finally, in Figure 3 (right), we compare the conservation errors in the computation of h, which is measured by

$$\left|\sum_j \overline{h}_j(t)\Delta x_j(t)-\sum_j \overline{h}_j(0)\Delta x_j(0)\right|.$$

As we have explained in Section 2.3, this conservation error is caused by the use of a quadrature in the approximation of cell averages of the bottom topography in (2.16). We have tested the trapezoidal and Simpson's rules and, as one can see in Figure 3 (right), the use of Simpson's rule leads to much smaller conservation errors.

Example 2 – Accuracy test

In this example, we experimentally check the order of accuracy of the proposed AMM central-upwind scheme. We take the following initial data and bottom topography:

$$w(x,y,0)\equiv 1,\quad u(x,y,0)\equiv 0.3,\quad v(x,y,0)\equiv 0,\quad B(x,y)=0.5e^{-25\left(x^2+2y^2\right)}.$$

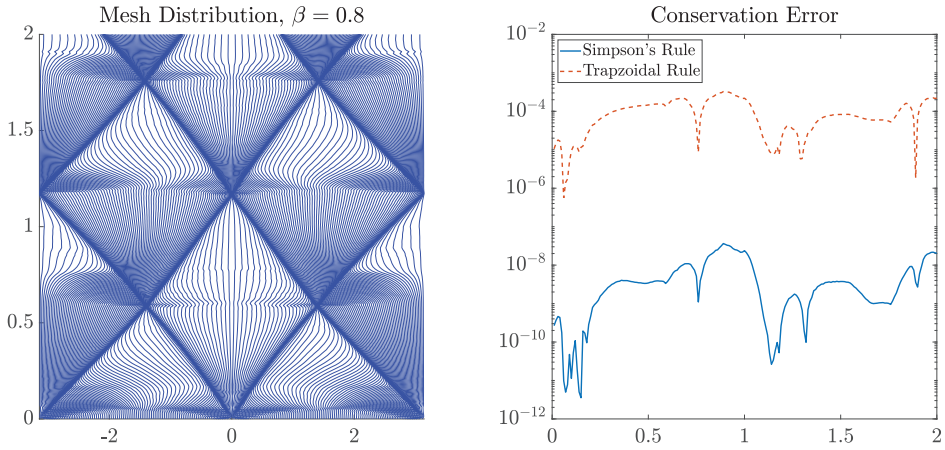

FIGURE 3. Example 1: Time-space distribution of mesh cells (*left*) and time evolution of the conservation errors in the computation of h (*right*).

TABLE 1. Example 2: The L^1-, L^2- and L^∞-errors and convergence rates for h.

N	L^1-error	Rate	L^2-error	Rate	L^∞-error	Rate
50	9.32E-05	–	1.25E-04	–	4.40E-04	–
100	3.04E-05	1.62	4.21E-05	1.57	1.46E-04	1.60
200	8.32E-06	1.87	1.16E-05	1.85	4.15E-05	1.81

The computational domain $[-1,1]\times[-0.5,0.5]$ is initially split into $N\times N$ uniform finite-volume cells and zero-order extrapolation is used at all boundaries.

We take $\beta = 0.5$ and compute a sequence of numerical solutions using $N = 50$, 100, 200 and 400 (with the 400×400 solution being used as the reference solution) until the final time $t = 0.07$, by which the solution remains smooth. In Table 1, we show the L^1-, L^2- and L^∞-norms of the errors in the computation of h together with the experimental rates of convergence. As one can see, the rates are close to 2 as expected.

Example 3 – Waves in a water tank

In this example, we consider the initial-boundary value problem (IBVP) for the 2-D Saint-Venant system in the computational domain $[-1,1]\times[-1,1]$ with the (reflective) solid wall boundary conditions. The bottom topography function is

$$B(x,y) = 0.25\, e^{-20\left(x^2+y^2\right)},$$

and the initial conditions are given by

$$w(x,y,0) = \begin{cases} 1, & (x+1)^2+(y+1)^2 < 0.25,\\ 1, & (x+1)^2+(y-1)^2 < 0.25,\\ 1, & (x-1)^2+y^2 < 0.25,\\ 0.5, & \text{otherwise,}\end{cases} \qquad u(x,y,0) = v(x,y,0) \equiv 0.$$

We initialy split the computational domain into 200×200 uniform finite-volume cells and solve the studied IBVP using the designed AMM central-upwind scheme. We choose the monitor function with $D\boldsymbol{U} = \Delta w$ in (2.11) and $\beta = 0.7$. The contour plots of w and the corresponding meshes at times $t = 0.125$, 0.25, 0.375 and 0.5

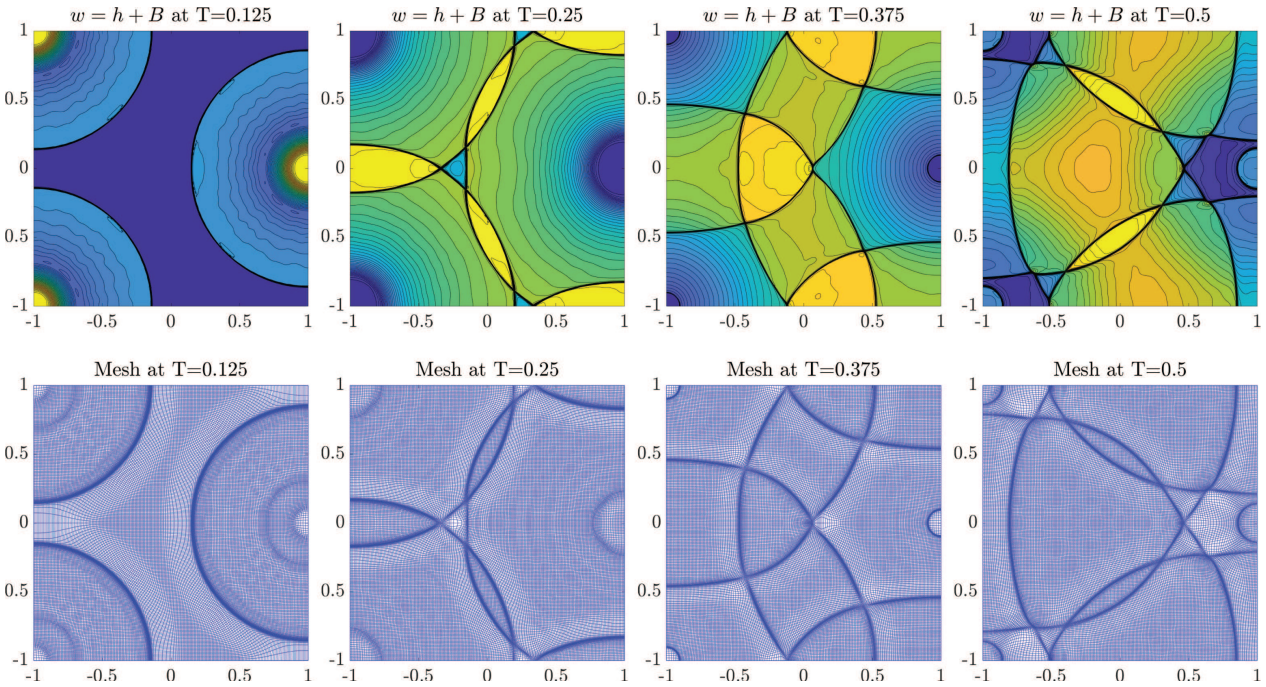

FIGURE 4. Example 3: Time evolution of w (*top row*) and the corresponding meshes (*bottom row*).

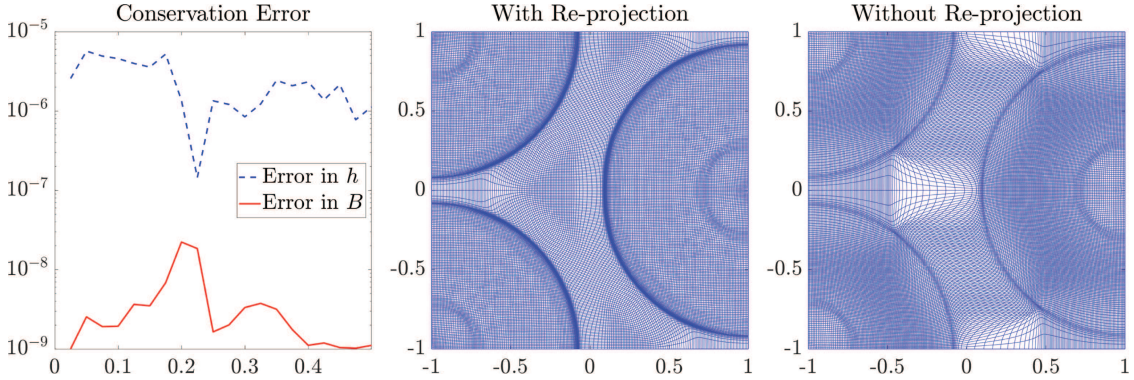

FIGURE 5. Example 3: Time evolution of the conservation errors in B and h (*left*); mesh distributions at $t = 0.15$ with (*middle*) and without (*right*) the re-projection process.

are presented in Figure 4. As one can see, the discontinuities in w are clearly captured by the proposed AMM method.

The re-projection (see Rem. 2.11) onto the uniform mesh has been performed at times $t = 0.025, 0.05, \ldots, 0.475, 0.5$, that is, every 0.025 s. This re-projection process leads to additional conservation errors, but it can significantly improve the quality of the mesh distribution. The time evolution of the conservation errors in h and B, as well as the comparison between meshes with/without this re-projection process at time $t = 0.15$ are shown in Figure 5. As one can see, without the re-projection procedure, a large portion of the grid

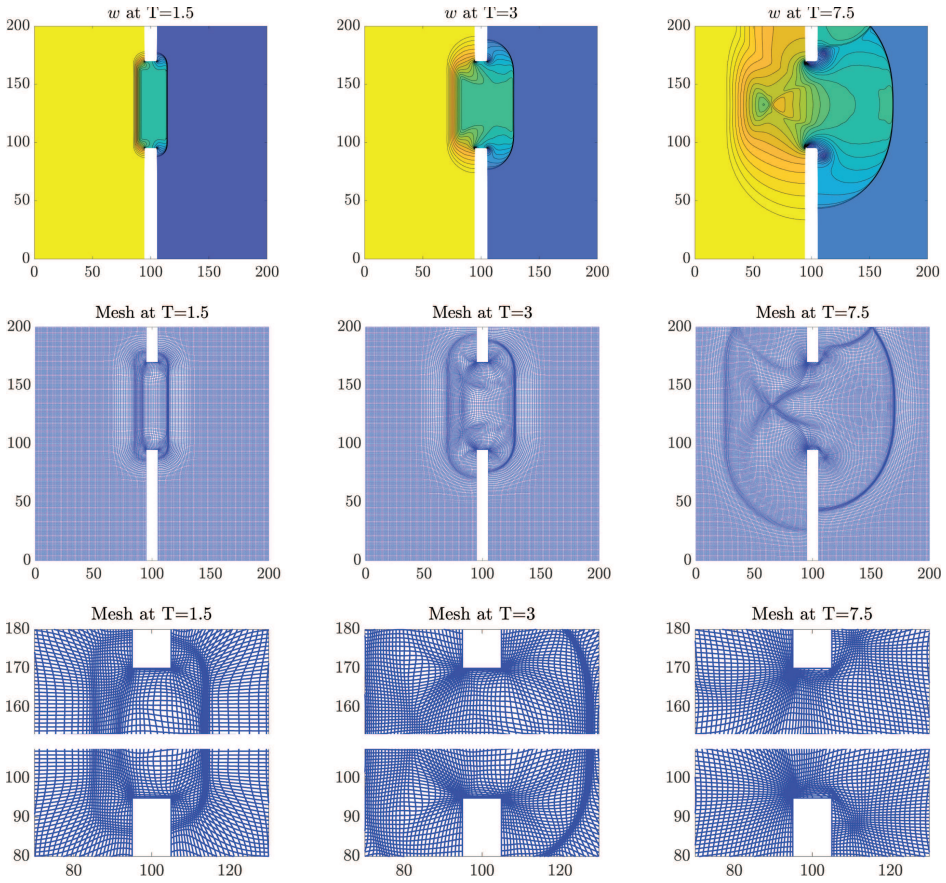

FIGURE 6. Example 4: Time evolution of w (*top row*) and the corresponding meshes (*middle row*) including zoom at $[70,130]\times[80,110]$ and $[70,130]\times[150,180]$ areas (*bottom row*).

points get trapped by the circular shocks, which leads to the lack of cells in the central part of the domain and thus prevents sharp resolution of shocks.

Example 4 – Asymmetric dam break

In this example, we test the designed scheme on a benchmark taken from [20]. The computational domain is $[0,95]\times[0,200]\cup[95,105]\times[95,180]\cup[105,200]\times[0,200]$ with the (reflective) solid wall boundary conditions, the bottom topography is flat ($B(x,y)\equiv 0$), and the initial conditions are given by

$$w(x,y,0)=\begin{cases}10, & x<100,\\ 5, & \text{otherwise},\end{cases}\qquad u(x,y,0)=v(x,y,0)\equiv 0.$$

We initially split the computational domain into the uniform Cartesian cells of size $\Delta x=\Delta y=1$ and solve the studied IBVP using the proposed AMM central-upwind scheme. During the moving mesh process, the vertices at the boundary are kept fixed and all of the other grid points initially located on the boundary are allowed to move according to the moving mesh equation, but only along the boundaries. We choose the monitor function with $D\boldsymbol{U}=\Delta w$ in (2.11) and $\beta=0.7$. The contour plots of w and the corresponding meshes at times $t=1.5$, 3 and 7.5 are presented in Figure 6. As one can see, the mesh is concentrated at the discontinuous and other rough parts of the solution, which is captured with an extremely high resolusion.

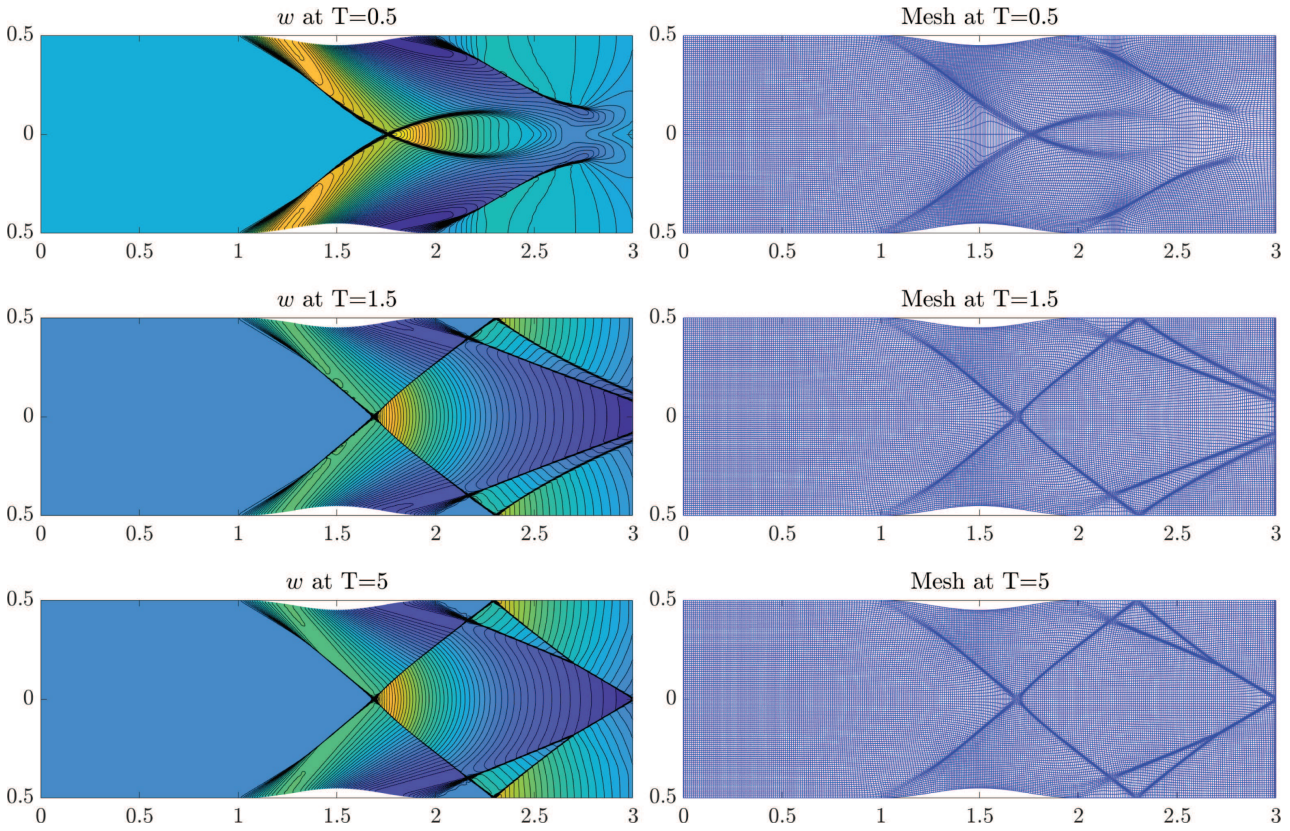

FIGURE 7. Example 5: Time evolution of w (*left column*) and the corresponding meshes (*right column*).

Example 5 – Flow in a converging-diverging channel

In this example, taken from [15] (see also [6]), we study water flow in an open converging-diverging channel of length 3 with a symmetric constriction of length 1 at the center. We consider the IBVP in the computational domain $[0,3]\times[-y_b(x),y_b(x)]$, where

$$y_b(x)=\begin{cases}0.5-0.05\cos^2(\pi(x-1.5)), & |x-1.5|<0.5,\\ 0.5, & \text{otherwise},\end{cases}$$

with the (reflective) solid wall boundary conditions, flat bottom topography ($B(x,y)\equiv 0$), and the following initial conditions:

$$w(x,y,0)\equiv 1,\quad u(x,y,0)\equiv 2,\quad v(x,y,0)\equiv 0.$$

The mesh is initialized as follows. We split the rectangular domain $[0,3]\times[-0.5,0.5]$ into 300×100 uniform finite-volume cells whose vertices are denoted by $\boldsymbol{z}^*_{j+\frac12,k+\frac12}=\left(x^*_{j+\frac12,k+\frac12},y^*_{j+\frac12,k+\frac12}\right)$, and project them onto the computational domain using

$$x_{j+\frac12,k+\frac12}=x^*_{j+\frac12,k+\frac12},\qquad y_{j+\frac12,k+\frac12}=2y_b\Big(x^*_{j+\frac12,k+\frac12}\Big)y^*_{j+\frac12,k+\frac12}.$$

We then solve the IBVP using the designed AMM central-upwind scheme. During the moving mesh process, the grid points initially located on the upper and lower boundaries are evolved in time by changing their x-

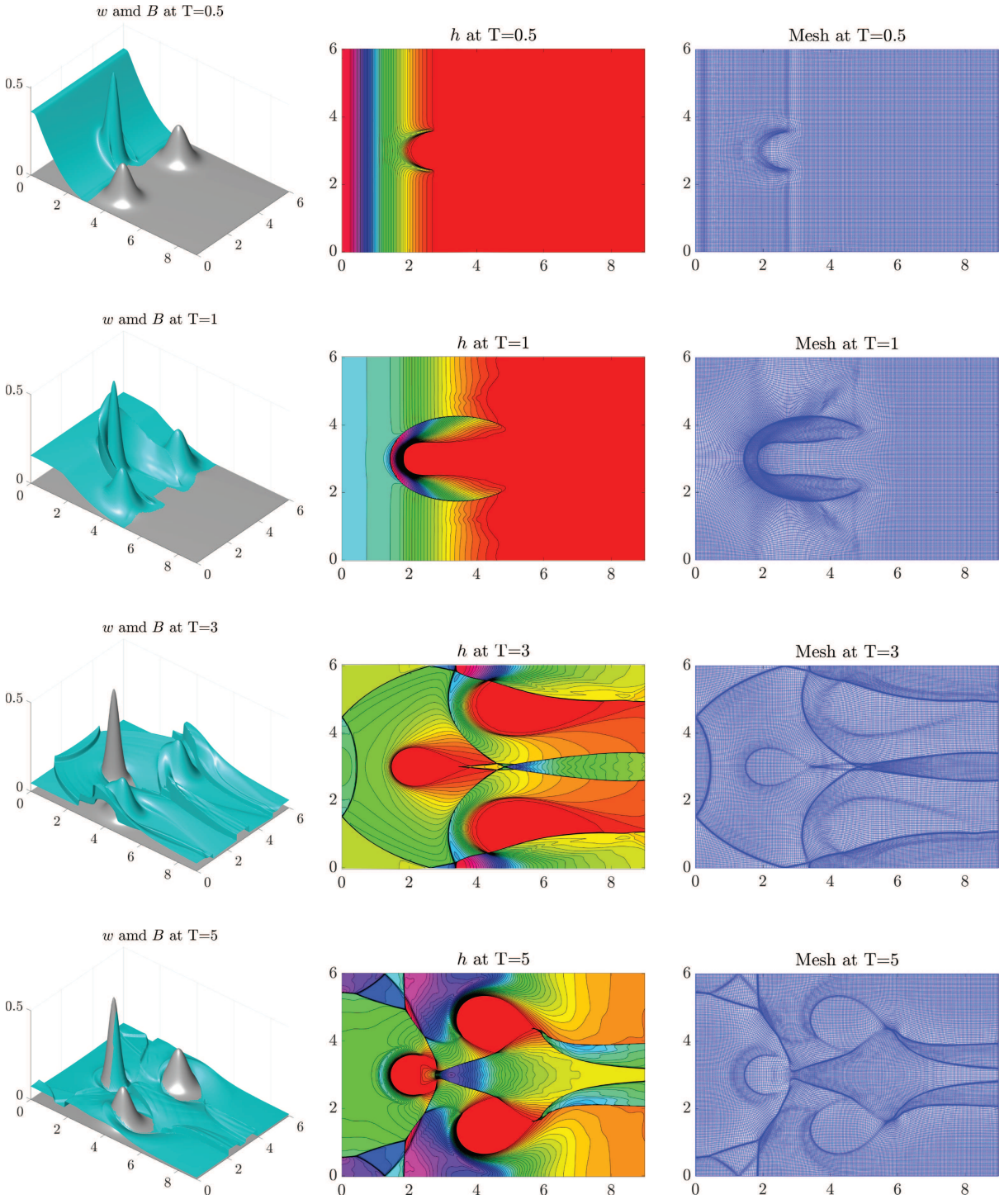

FIGURE 8. Example 6: Time evolution of w (plotted together with B in the *left column*), h (*middle column*) and the corresponding meshes (*right column*).

coordinates according to the moving mesh equation, while their y-coordinates are computed using the boundary function $y = y_b(x)$ in order to keep these grid points on the corresponding parts of the boundary. We choose the monitor function with $D\boldsymbol{U} = \Delta w$ in (2.11) and $\beta = 0.2$. The contour plots of w and the corresponding meshes at times $t = 0.5$, 1.5 and 5 are presented in Figure 7. As one can see, the solution, including the steady state reached by time $t = 5$, has been accurately captured by the proposed AMM central-upwind scheme and the mesh is automatically adjusted to the computed solution structure.

Example 6 – Dam break with wet/dry front

In the final example, we consider a dam-break example over the domain with a nonflat bottom topography and initially dry areas. We study the IBVP in the computational domain $[0,9]\times[0,6]$ with the (reflective) solid wall boundary conditions at $x = 0$, $y = 0$ and $y = 6$ and an open boundary at $x = 9$. The bottom topography contains three exponential humps:

$$B(x,y) = 0.5\ e^{-8(x-2)^2-10(y-3)^2} + 0.2\ e^{-3(x-4)^2-4(y-1.2)^2} + 0.2\ e^{-3(x-4)^2-4(y-4.8)^2},$$

and the initial conditions are given by

$$w(x,y,0) = \begin{cases} 0.5, & x < 0.9,\\ B(x,y), & \text{otherwise,}\end{cases} \qquad u(x,y,0) = v(x,y,0) \equiv 0.$$

We initially split the computational domain into 300×200 uniform Cartesian cells and solve the studied IBVP using the proposed AMM central-upwind scheme. We choose the monitor function with $D\boldsymbol{U} = \Delta h$ in (2.11) and $\beta = 0.3$. In Figure 8, we show the time evolution of the dam-break wave propagating over the initially dry bed together with the corresponding meshes. It can be observed that as in previous examples, the designed scheme sharply captures a complicated wave structure and, in addition, the scheme performs well when handling both wetting and drying processes.

Appendix A. Proof of Theorem 2.5

We consider several different cases depending on where the cell C_j is located in.

Case 1 (C_j as well as C_{j-1} and C_{j+1} are "wet"). In this case, equation (2.17) reduces to (2.15). Moreover, since we reconstruct w (not h) in the cell C_j, we have $\overline{w}_j^{\,\nu} = \frac{1}{2}\Big(w^-_{j+\frac12} + w^+_{j-\frac12}\Big)$, which after being substituted into (2.15) gives

$$\Delta x_j^{\nu+1}\overline{w}_j^{\,\nu+1} = \begin{cases} \dfrac{\Delta x_j^\nu}{2}\Big(w^-_{j+\frac12} + w^+_{j-\frac12}\Big) + \mu^{\nu+\frac12}_{j+\frac12}w^+_{j+\frac12} - \mu^{\nu+\frac12}_{j-\frac12}w^-_{j-\frac12}, & \text{if } \mu^{\nu+\frac12}_{j+\frac12} > 0,\ \mu^{\nu+\frac12}_{j-\frac12} < 0,\\ \dfrac{\Delta x_j^\nu}{2}w^+_{j-\frac12} + \Big(\dfrac{\Delta x_j^\nu}{2} + \mu^{\nu+\frac12}_{j+\frac12}\Big)w^-_{j+\frac12} - \mu^{\nu+\frac12}_{j-\frac12}w^-_{j-\frac12}, & \text{if } \mu^{\nu+\frac12}_{j+\frac12} < 0,\ \mu^{\nu+\frac12}_{j-\frac12} < 0,\\ \dfrac{\Delta x_j^\nu}{2}w^-_{j+\frac12} + \mu^{\nu+\frac12}_{j+\frac12}w^+_{j+\frac12} + \Big(\dfrac{\Delta x_j^\nu}{2} - \mu^{\nu+\frac12}_{j-\frac12}\Big)w^+_{j-\frac12}, & \text{if } \mu^{\nu+\frac12}_{j+\frac12} > 0,\ \mu^{\nu+\frac12}_{j-\frac12} > 0,\\ \Big(\dfrac{\Delta x_j^\nu}{2} + \mu^{\nu+\frac12}_{j+\frac12}\Big)w^-_{j+\frac12} + \Big(\dfrac{\Delta x_j^\nu}{2} - \mu^{\nu+\frac12}_{j-\frac12}\Big)w^+_{j-\frac12}, & \text{if } \mu^{\nu+\frac12}_{j+\frac12} < 0,\ \mu^{\nu+\frac12}_{j-\frac12} > 0. \end{cases} \tag{A.1}$$

Due to the relaxation step (2.12), we have $\frac{\Delta x_j^\nu}{2} + \mu^{\nu+\frac12}_{j+\frac12} \ge 0$ and $\frac{\Delta x_j^\nu}{2} - \mu^{\nu+\frac12}_{j-\frac12} \ge 0$, which together with the identity $\Delta x_j^{\nu+1} = \Delta x_j^\nu + \mu^{\nu+\frac12}_{j+\frac12} - \mu^{\nu+\frac12}_{j-\frac12}$ imply that $\overline{w}_j^{\,\nu+1}$ is a convex combination of $\Big(w^\pm_{j\pm\frac12}\Big)^\nu$, which, in turn, guarantees that

$$\overline{w}_j^{\,\nu+1} \ge \min\Big\{w^\nu_{j+\frac12}, w^\nu_{j-\frac12}\Big\} \ge \min\big\{\overline{w}_j^{\,\nu}, \overline{w}^\nu_{j+1}, \overline{w}^\nu_{j-1}\big\}, \tag{A.2}$$

where $w^{\nu}_{j+\frac12}$ is defined in (2.14) and the latter inequality is true since this is a property of the piecewise linear reconstruction used in Section 2.1.1. We now note that since the condition (2.6) is not satisfied in the "wet" area, we have

$$\min\left\{\overline{w}^{\nu}_{j},\overline{w}^{\nu}_{j+1},\overline{w}^{\nu}_{j-1}\right\}\geq\max_{x\in\left(x^{\nu}_{j-1},x^{\nu}_{j+1}\right)}B(x)\geq\max_{x\in\left(x^{\nu+1}_{j-\frac12},x^{\nu+1}_{j+\frac12}\right)}B(x),\tag{A.3}$$

where the latter inequality is guaranteed by (2.13). Thus, the inequality (2.20) immediately follows from (A.2) and (A.3).

Case 2 (C_j as well as C_{j-1} and C_{j+1} are "dry"). In this case, we reconstruct h (not w) in the cell C_j, and thus we have $\overline{h}^{\nu}_{j}=\frac12\left(h^{-}_{j+\frac12}+h^{+}_{j-\frac12}\right)$. Using this and the fact that $\overline{w}^{\nu}_{j}=\overline{h}^{\nu}_{j}+\overline{B}^{\nu}_{j}$, we rewrite (2.17) as follows:

$$\begin{aligned}\Delta x^{\nu+1}_{j}\overline{w}^{\nu+1}_{j}&=\Delta x^{\nu}_{j}\left(\overline{h}^{\nu}_{j}+\overline{B}^{\nu}_{j}\right)+\mu^{\nu+\frac12}_{j+\frac12}\left(h^{\nu}_{j+\frac12}+\overline{B}^{\nu+\frac12}_{j+\frac12}\right)-\mu^{\nu+\frac12}_{j-\frac12}\left(h^{\nu}_{j-\frac12}+\overline{B}^{\nu+\frac12}_{j-\frac12}\right)+B^{\rm corr}_{j}\\&=\Delta x^{\nu}_{j}\overline{h}^{\nu}_{j}+\mu^{\nu+\frac12}_{j+\frac12}h^{\nu}_{j+\frac12}-\mu^{\nu+\frac12}_{j-\frac12}h^{\nu}_{j-\frac12}+\Delta x^{\nu+1}_{j}\overline{B}^{\nu+1}_{j}=\Delta x^{\nu+1}_{j}\overline{h}^{\nu+1}_{j,1}+\Delta x^{\nu+1}_{j}\overline{B}^{\nu+1}_{j},\end{aligned}$$

where we have used the following notation:

$$\overline{h}^{\nu+1}_{j,1}:=\frac{1}{\Delta x^{\nu+1}_{j}}\left(\Delta x^{\nu}_{j}\overline{h}^{\nu}_{j}+\mu^{\nu+\frac12}_{j+\frac12}h^{\nu}_{j+\frac12}-\mu^{\nu+\frac12}_{j-\frac12}h^{\nu}_{j-\frac12}\right).$$

Using (2.14), this equation can be rewritten as (compare with (A.1)):

$$\Delta x^{\nu+1}_{j}\overline{h}^{\nu+1}_{j,1}=\begin{cases}\dfrac{\Delta x^{\nu}_{j}}{2}\left(h^{-}_{j+\frac12}+h^{+}_{j-\frac12}\right)+\mu^{\nu+\frac12}_{j+\frac12}h^{+}_{j+\frac12}-\mu^{\nu+\frac12}_{j-\frac12}h^{-}_{j-\frac12}, & \text{if } \mu^{\nu+\frac12}_{\rm j+\frac12}>0,\ \mu^{\nu+\frac12}_{\rm j-\frac12}<0,\\ \dfrac{\Delta x^{\nu}_{j}}{2}h^{+}_{j-\frac12}+\left(\dfrac{\Delta x^{\nu}_{j}}{2}+\mu^{\nu+\frac12}_{j+\frac12}\right)h^{-}_{j+\frac12}-\mu^{\nu+\frac12}_{j-\frac12}h^{-}_{j-\frac12}, & \text{if } \mu^{\nu+\frac12}_{\rm j+\frac12}<0,\ \mu^{\nu+\frac12}_{\rm j-\frac12}<0,\\ \dfrac{\Delta x^{\nu}_{j}}{2}h^{-}_{j+\frac12}+\mu^{\nu+\frac12}_{j+\frac12}h^{+}_{j+\frac12}+\left(\dfrac{\Delta x^{\nu}_{j}}{2}-\mu^{\nu+\frac12}_{j-\frac12}\right)h^{+}_{j-\frac12}, & \text{if } \mu^{\nu+\frac12}_{\rm j+\frac12}>0,\ \mu^{\nu+\frac12}_{\rm j-\frac12}>0,\\ \left(\dfrac{\Delta x^{\nu}_{j}}{2}+\mu^{\nu+\frac12}_{j+\frac12}\right)h^{-}_{j+\frac12}+\left(\dfrac{\Delta x^{\nu}_{j}}{2}-\mu^{\nu+\frac12}_{j-\frac12}\right)h^{+}_{j-\frac12}, & \text{if } \mu^{\nu+\frac12}_{\rm j+\frac12}<0,\ \mu^{\nu+\frac12}_{\rm j-\frac12}>0.\end{cases}$$

Similarly to Case 1, we conclude that $\overline{h}^{\nu+1}_{j,1}$ is a convex combination of $\left(h^{\pm}_{j\pm\frac12}\right)^{\nu}$, which are nonnegative since the reconstruction of h is positivity preserving. Therefore, $\overline{h}^{\nu+1}_{j,1}\geq0$ and thus (A.2) is satisfied.

Case 3 (C_j is "wet", while C_{j+1} or C_{j-1} or both are "dry"). In this case, the cell C_j is located near the wetting/drying interface and the projection procedure depends on the type of the neighbouring cells and also on whether the cell interface moves into the "wet" or "dry" area. We will first consider the situation with only one "dry" neighbor, say, C_{j+1} (Case 3a) and then we will consider the case when C_j is an isolated "wet" cell (Case 3b).

Case 3a (C_{j-1} and C_j are "wet", while C_{j+1} is "dry"). There are two possible situations: either the interface $x^{\nu}_{j+\frac12}$ moves to the left $\left(\mu^{\nu+\frac12}_{j+\frac12}<0\right)$ into the "wet" area or to the right $\left(\mu^{\nu+\frac12}_{j+\frac12}>0\right)$ into the "dry" area. In the former situation, the proof is identical to Case 1. We therefore consider the case $\mu^{\nu+\frac12}_{j+\frac12}>0$ and use (2.14) to reduce (2.17) to

$$\Delta x^{\nu+1}_{j}\overline{w}^{\nu+1}_{j}=\Delta x^{\nu}_{j}\overline{w}^{\nu}_{j}+\mu^{\nu+\frac12}_{j+\frac12}\left(h^{+}_{j+\frac12}+\overline{B}^{\nu+\frac12}_{j+\frac12}\right)-\mu^{\nu+\frac12}_{j-\frac12}w^{\nu}_{j-\frac12},$$

and then rewrite it as

$$\Delta x_j^{\nu+1}\overline{w}_j^{\nu+1}=\begin{cases}\Delta x_j^{\nu}\overline{w}_j^{\nu}+\mu_{j+\frac12}^{\nu+\frac12}\left(h_{j+\frac12}^{+}+\bar{B}_{j+\frac12}^{\nu+\frac12}\right)-\mu_{j-\frac12}^{\nu+\frac12}w_{j-\frac12}^{-}, & \text{if } \mu_{j-\frac12}^{\nu+\frac12}<0,\\ \dfrac{\Delta x_j^{\nu}}{2}w_{j+\frac12}^{-}+\mu_{j+\frac12}^{\nu+\frac12}(h_{j+\frac12}^{+}+\bar{B}_{j+\frac12}^{\nu+\frac12})+\left(\dfrac{\Delta x_j^{\nu}}{2}-\mu_{j-\frac12}^{\nu+\frac12}\right)w_{j-\frac12}^{+}, & \text{if } \mu_{j-\frac12}^{\nu+\frac12}>0.\end{cases}\tag{A.4}$$

We now denote by $B_j^{\max}:=\max_{x\in(x_{j-1}^{\nu},x_{j+1}^{\nu})}B(x)$ and note that since C_{j-1} and C_j are "wet" and we use the maximum principle preserving reconstruction of w in these cells, $\overline{w}_j^{\nu}\ge B_j^{\max}$, $w_{j-\frac12}^{\pm}\ge B_j^{\max}$ and $w_{j+\frac12}^{-}\ge B_j^{\max}$. We also note that since the reconstruction of h is positivity preserving, $h_{j+\frac12}^{+}\ge 0$, and that due to the relaxatoin step (2.12), we have $\frac{\Delta x_j^{\nu}}{2}-\mu_{j-\frac12}^{\nu+\frac12}\ge 0$. The desired bound (2.20) is then obtained by estimating the right-hand side (RHS) of (A.4) as follows:

$$\begin{aligned}\overline{w}_j^{\nu+1}&\ge\frac{1}{\Delta x_j^{\nu+1}}\left[\left(\Delta x_j^{\nu}-\mu_{j-\frac12}^{\nu+\frac12}\right)B_j^{\max}+\mu_{j+\frac12}^{\nu+\frac12}\bar{B}_{j+\frac12}^{\nu+\frac12}\right]=\frac{1}{\Delta x_j^{\nu+1}}\left[\left(x_{j+\frac12}^{\nu}-x_{j-\frac12}^{\nu+1}\right)B_j^{\max}+\int_{x_{j+\frac12}^{\nu}}^{x_{j+\frac12}^{\nu+1}}B(x)\,\mathrm{d}x\right]\\&\ge\frac{1}{\Delta x_j^{\nu+1}}\left(\int_{x_{j-\frac12}^{\nu+1}}^{x_{j+\frac12}^{\nu}}B(x)\,\mathrm{d}x+\int_{x_{j+\frac12}^{\nu}}^{x_{j+\frac12}^{\nu+1}}B(x)\,\mathrm{d}x\right)=\bar{B}_j^{\nu+1}.\end{aligned}$$

Case 3b (C_j is "wet", while both C_{j-1} and C_{j+1} are "dry"). The only situation in which the projection step is different from the one that have been already investigated, is when both interfaces of the cell C_j propagate into the "dry" areas, that is, when $\mu_{j-\frac12}^{\nu+\frac12}<0$ and $\mu_{j+\frac12}^{\nu+\frac12}>0$. In this case, we once again use (2.14) so that (2.17) reduces to

$$\Delta x_j^{\nu+1}\overline{w}_j^{\nu+1}=\Delta x_j^{\nu}\overline{w}_j^{\nu}+\mu_{j+\frac12}^{\nu+\frac12}\left(h_{j+\frac12}^{+}+\bar{B}_{j+\frac12}^{\nu+\frac12}\right)-\mu_{j-\frac12}^{\nu+\frac12}\left(h_{j-\frac12}^{-}+\bar{B}_{j-\frac12}^{\nu+\frac12}\right),$$

from which we obtain (2.20) using the fact that $\overline{w}_j^{\nu}\ge\bar{B}_j^{\nu}$, $h_{j+\frac12}^{+}\ge 0$ and $h_{j-\frac12}^{-}\ge 0$, namely:

$$\overline{w}_j^{\nu+1}\ge\frac{1}{\Delta x_j^{\nu+1}}\left(\Delta x_j^{\nu}\,\bar{B}_j^{\nu}+\int_{x_{j+\frac12}^{\nu}}^{x_{j+\frac12}^{\nu+1}}B(x)\,\mathrm{d}x+\int_{x_{j-\frac12}^{\nu+1}}^{x_{j-\frac12}^{\nu}}B(x)\,\mathrm{d}x\right)=\frac{1}{\Delta x_j^{\nu+1}}\int_{x_{j-\frac12}^{\nu+1}}^{x_{j+\frac12}^{\nu+1}}B(x)\,\mathrm{d}x=\bar{B}_j^{\nu+1}.$$

Case 4 (C_j is "dry", while C_{j+1} or C_{j-1} or both are "wet"). As in Case 3, the cell C_j is located at the wetting/drying interface and the projection procedure depends on the type of the neighbouring cells and also on whether the cell interface moves into the "wet" or "dry" area. We will first consider the situation with only one "wet" neighbor, say, C_{j+1} (Case 4a) and then we will consider the case when C_j is an isolated "dry" cell (Case 4b).

Case 4a (C_{j-1} and C_j are "dry", while C_{j+1} is "wet"). There are two possible situations: either the interface $x_{j+\frac12}^{\nu}$ moves to the left $\left(\mu_{j+\frac12}^{\nu+\frac12}<0\right)$ into the "dry" area or to the right $\left(\mu_{j+\frac12}^{\nu+\frac12}>0\right)$ into the "wet" area. In the former situation, the proof is identical to Case 2. We therefore consider the case $\mu_{j+\frac12}^{\nu+\frac12}>0$, in which (2.17) becomes

$$\begin{aligned}\Delta x_j^{\nu+1}\overline{w}_j^{\nu+1}&=\Delta x_j^{\nu}\left(\bar{h}_j^{\nu}+\bar{B}_j^{\nu}\right)+\mu_{j+\frac12}^{\nu+\frac12}w_{j+\frac12}^{+}-\mu_{j-\frac12}^{\nu+\frac12}\left(h_{j-\frac12}^{\nu}+\bar{B}_{j-\frac12}^{\nu+\frac12}\right)+B_j^{\mathrm{corr}}\\&=\Delta x_j^{\nu}\bar{h}_j^{\nu}+\mu_{j+\frac12}^{\nu+\frac12}\left(w_{j+\frac12}^{+}-\bar{B}_{j+\frac12}^{\nu+\frac12}\right)-\mu_{j-\frac12}^{\nu+\frac12}h_{j-\frac12}^{\nu}+\Delta x_j^{\nu+1}\bar{B}_j^{\nu+1}=\Delta x_j^{\nu+1}\bar{h}_{j,2}^{\nu+1}+\Delta x_j^{\nu+1}\bar{B}_j^{\nu+1},\end{aligned}$$

where we have used (2.14) and the fact that $\overline{w}_j^{\nu}=\overline{h}_j^{\nu}+\overline{B}_j^{\nu}$ and introduced the following notation:

$$\overline{h}_{j,2}^{\nu+1}:=\frac{1}{\Delta x_j^{\nu+1}}\Big(\Delta x_j^{\nu}\overline{h}_j^{\nu}+\mu_{j+\frac12}^{\nu+\frac12}\Big(w_{j+\frac12}^{+}-\overline{B}_{j+\frac12}^{\nu+\frac12}\Big)-\mu_{j-\frac12}^{\nu+\frac12}h_{j-\frac12}^{\nu}\Big).$$

Taking into account (2.14), the last equation can be rewritten as:

$$\Delta x_j^{\nu+1}\overline{h}_{j,2}^{\nu+1}=\begin{cases}\dfrac{\Delta x_j^{\nu}}{2}h_{j+\frac12}^{-}+\mu_{j+\frac12}^{\nu+\frac12}\Big(w_{j+\frac12}^{+}-\overline{B}_{j+\frac12}^{\nu+\frac12}\Big)+\Big(\dfrac{\Delta x_j^{\nu}}{2}-\mu_{j-\frac12}^{\nu+\frac12}\Big)h_{j-\frac12}^{+}, & \text{if } \mu_{j-\frac12}^{\nu+\frac12}>0,\\ \dfrac{\Delta x_j^{\nu}}{2}\Big(h_{j-\frac12}^{+}+h_{j+\frac12}^{-}\Big)+\mu_{j+\frac12}^{\nu+\frac12}\Big(w_{j+\frac12}^{+}-\overline{B}_{j+\frac12}^{\nu+\frac12}\Big)-\mu_{j-\frac12}^{\nu+\frac12}h_{j-\frac12}^{-}, & \text{if } \mu_{j-\frac12}^{\nu+\frac12}<0.\end{cases}$$

Since the piecewise linear reconstruction of w satisfies the right inequality in (A.2) and the cell C_{j+1} is "wet", we have

$$w_{j+\frac12}^{+}\ge\min\big\{\overline{w}_j^{\nu},\overline{w}_{j+1}^{\nu}\big\}\ge\min\big\{\overline{w}_j^{\nu},\overline{w}_{j+1}^{\nu},\overline{w}_{j+2}^{\nu}\big\}\overset{(2.6)}{\ge}\max_{x\in\left(x_j^{\nu},x_{j+2}^{\nu}\right)}B(x)\overset{(2.12)}{\ge}\max_{x\in\left(x_{j+\frac12}^{\nu},\,x_{j+\frac12}^{\nu+1}\right)}B(x)\overset{(2.18)}{\ge}\overline{B}_{j+\frac12}^{\nu+\frac12}.$$

Next, due to the relaxation step (2.12), we have $\frac{\Delta x_j^{\nu}}{2}-\mu_{j-\frac12}^{\nu+\frac12}\ge0$, which together with the identity $\Delta x_j^{\nu+1}=\Delta x_j^{\nu}+\mu_{j+\frac12}^{\nu+\frac12}-\mu_{j-\frac12}^{\nu+\frac12}$ and positivity preserving property of the reconstruction of h imply that $\overline{h}_j^{\nu+1}$ is a convex combination of $(h_{j\pm\frac12}^{\pm})^{\nu}$ and $w_{j+\frac12}^{+}-B_{j+\frac12}^{\nu+\frac12}$. Therefore, $\overline{h}_{j,2}^{\nu+1}\ge0$ and thus (2.20) is satisfied.

Case 4b (C_j is "dry", while both C_{j-1} and C_{j+1} are "wet"). The only situation in which the projection step is different from the one that have been already investigated, is when both interfaces of the cell C_j propagate into the "wet" areas, that is, when $\mu_{j-\frac12}^{\nu+\frac12}<0$ and $\mu_{j+\frac12}^{\nu+\frac12}>0$. In this case, we use (2.14) and the fact that $\overline{w}_j^{\nu}=\overline{h}_j^{\nu}+\overline{B}_j^{\nu}$ to rewrite as

$$\begin{aligned}\Delta x_j^{\nu+1}\overline{w}_j^{\nu+1}&=\Delta x_j^{\nu}\Big(\overline{h}_j^{\nu}+\overline{B}_j^{\nu}\Big)+\mu_{j+\frac12}^{\nu+\frac12}w_{j+\frac12}^{+}-\mu_{j-\frac12}^{\nu+\frac12}w_{j-\frac12}^{-}+B_j^{\text{corr}}\\&=\Delta x_j^{\nu}\overline{h}_j^{\nu}+\mu_{j+\frac12}^{\nu+\frac12}\Big(w_{j+\frac12}^{+}-\overline{B}_{j+\frac12}^{\nu+\frac12}\Big)-\mu_{j-\frac12}^{\nu+\frac12}\Big(w_{j-\frac12}^{-}-\overline{B}_{j-\frac12}^{\nu+\frac12}\Big)+\Delta x_j^{\nu+1}\overline{B}_j^{\nu+1}\\&=\Delta x_j^{\nu+1}\overline{h}_{j,3}^{\nu+1}+\Delta x_j^{\nu+1}\overline{B}_j^{\nu+1},\end{aligned}$$

where we have used the following notation:

$$\overline{h}_{j,3}^{\nu+1}:=\frac{1}{\Delta x_j^{\nu+1}}\Big(\Delta x_j^{\nu}\overline{h}_j^{\nu}+\mu_{j+\frac12}^{\nu+\frac12}\Big(w_{j+\frac12}^{+}-\overline{B}_{j+\frac12}^{\nu+\frac12}\Big)-\mu_{j-\frac12}^{\nu+\frac12}\Big(w_{j-\frac12}^{-}-\overline{B}_{j-\frac12}^{\nu+\frac12}\Big)\Big).$$

Similarly to Case 3a, we note that since piecewise linear reconstruction of w satisfies the right inequality in (A.2) and the cells C_{j-1} and C_{j+1} are "wet", we have $w_{j-\frac12}^{-}-\overline{B}_{j-\frac12}^{\nu+\frac12}\ge0$ and $w_{j+\frac12}^{+}-\overline{B}_{j+\frac12}^{\nu+\frac12}\ge0$, which, together with the identity $\Delta x_j^{\nu+1}=\Delta x_j^{\nu}+\mu_{j+\frac12}^{\nu+\frac12}-\mu_{j-\frac12}^{\nu+\frac12}$, imply that $\overline{h}_{j,3}^{\nu+1}$ is a convex combination of $\overline{h}_j^{\nu}$, $w_{j-\frac12}^{-}-\overline{B}_{j-\frac12}^{\nu+\frac12}$ and $w_{j+\frac12}^{+}-\overline{B}_{j+\frac12}^{\nu+\frac12}$. Therefore, we conclude that $\overline{h}_{j,3}^{\nu+1}\ge0$ and the inequality (2.20) immediately follows.

Appendix B. Quadrature for general quadrilaterals

In this appendix, we provide a detailed description of the 2-D quadrature over quadrilaterals, which was used in our numerical experiments. Here, we consider a general quadrilateral $ABCD$, which may be convex, concave

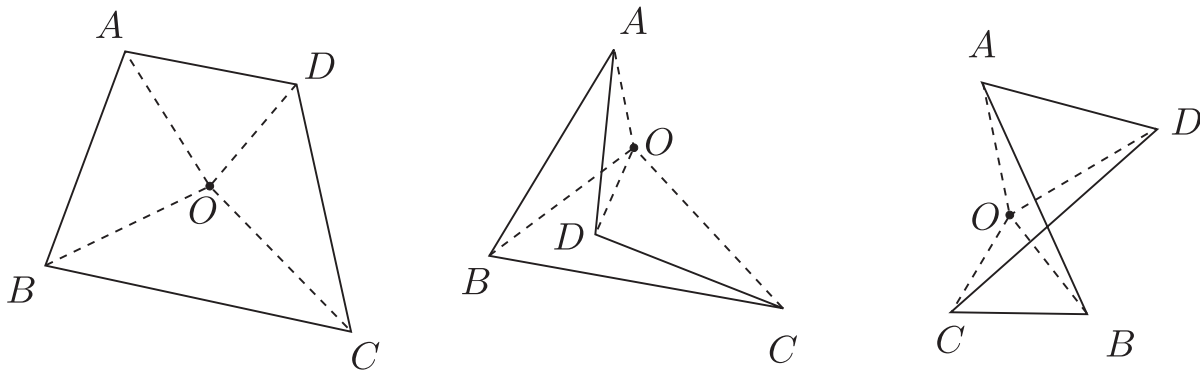

FIGURE B.1. Convex (*left*), concave (*middle*) and self-intersecting (*right*) quadrilaterals.

or even self-intersecting; see Figure B.1. We set $O := \frac{1}{4}(A+B+C+D)$ and split the quadrilateral into four triangles and then we define a signed integral by

$$\begin{aligned}\iint_{ABCD} f(x,y)\,\mathrm{d}x\,\mathrm{d}y := \pm\iint_{OAB} f(x,y)\,\mathrm{d}x\,\mathrm{d}y \pm \iint_{OBC} f(x,y)\,\mathrm{d}x\,\mathrm{d}y\\ \pm\iint_{OCD} f(x,y)\,\mathrm{d}x\,\mathrm{d}y \pm \iint_{ODA} f(x,y)\,\mathrm{d}x\,\mathrm{d}y,\end{aligned} \tag{B.1}$$

where the sign in front of each of the integrals on the RHS of (B.1) is "+" if the verticies of the triangle are listed in the counterclockwise order, and "−" otherwise.

We then approximate the integrals over each of the triangles using a 7-point Gaussian quadrature, for example,

$$\iint_{\Delta_{OAB}} f(x,y)\,\mathrm{d}x\,\mathrm{d}y \approx \left|\overrightarrow{OA}\times\overrightarrow{OB}\right|\left(\frac{f(O)+f(A)+f(B)}{40}+\frac{f(M_{OA})+f(M_{OB})+f(M_{AB})}{15}+\frac{9}{40}f\big(O^{\mathrm{CM}}\big)\right),$$

where M_{OA}, M_{OB} and M_{AB} are the midpoints of the corresponding edges of the triangle OAB and O^{CM} is its center of mass.

APPENDIX C. POSITIVITY ENSURING CFL CONDITIONS

In this appendix, we derive the CFL conditions, which ensure the positivity of h during the time evolution without applying the draining time-step technique introduced in Sections 2.1.3 and 2.4.4 in the 1-D and 2-D cases, respectively.

C.1. One-dimensional CFL condition

We first note that if the cell C_j is "wet", the cell average $\overline{B}_j$ in (2.16) (we omit the upper index ν for the sake of brevity) is obtained using a quadrature. If the trapezoidal rule is used, then $\overline{B}_j = \Big(B_{j+\frac12}+B_{j-\frac12}\Big)/2$ and

$$\overline{h}_j = \overline{w}_j - \overline{B}_j = \frac12\Big(w^-_{j+\frac12}+w^+_{j-\frac12}-\Big(B_{j+\frac12}+B_{j-\frac12}\Big)\Big) = \frac12\Big(h^-_{j+\frac12}+h^+_{j-\frac12}\Big).$$

If Simpson's rule is used, then $\overline{B}_j = \Big(B_{j+\frac12}+4B_j+B_{j-\frac12}\Big)/6$ and

$$\overline{h}_j = \frac16\Big(w^-_{j+\frac12}-B_{j+\frac12}+4(\overline{w}_j-B_j)+w^+_{j-\frac12}-B_{j-\frac12}\Big) \ge \frac16\Big(h^-_{j+\frac12}+h^+_{j-\frac12}\Big), \tag{C.1}$$

where $B_j := B(x_j)$ and we have used the fact that for a piecewise linear reconstruction of w, $w_j = \overline{w}_j$, Simpson's rule is exact, and thus $\overline{w}_j = \left(w^-_{j+\frac12} + 4\overline{w}_j + w^+_{j-\frac12}\right)/6$. Notice that in order to establish the inequality (C.1), one needs to use the inequality $\overline{w}_j \geq B_j$. In the cells, where the latter inequality is not true, that is, where $\overline{w}_j < B_j$, or in "dry" cells defined in (2.6), (2.7), we reconstruct h instead of w and this approach gives

$$\overline{h}_j = \frac12\left(h^-_{j+\frac12} + h^+_{j-\frac12}\right).$$

We now prove the following theorem.

Theorem C.1. *Let h is evolved in time using the forward Euler discretization (2.10). If $\overline{h}_j(t) \geq 0$ for all j, and the time step satisfies the following CFL condition:*

$$\Delta t \leq \alpha \min_j \left\{ \frac{\Delta x_j}{a^+_{j+\frac12}}, \frac{\Delta x_j}{\left|a^-_{j-\frac12}\right|} \right\},$$

where $\alpha = 1/2$ if $\overline{B}_j$ is computed using the trapezoidal rule and $\alpha = 1/6$ if Simpson's rule is used, then $\overline{h}_j(t+\Delta t) \geq 0$ for all j.

Proof. First, we use (2.4) and rewrite the central-upwind numerical flux as follows:

$$\begin{aligned} H^{(1)}_{j+\frac12} &= \frac{a^+_{j+\frac12}h^-_{j+\frac12}u^-_{j+\frac12} - a^-_{j+\frac12}h^+_{j+\frac12}u^+_{j+\frac12} + a^+_{j+\frac12}a^-_{j+\frac12}\left[h^+_{j+\frac12} - h^-_{j+\frac12}\right]}{a^+_{j+\frac12} - a^-_{j+\frac12}} \\ &= \frac{h^-_{j+\frac12}a^+_{j+\frac12}\left(u^-_{j+\frac12} - a^-_{j+\frac12}\right) - h^+_{j+\frac12}a^-_{j+\frac12}\left(u^+_{j+\frac12} - a^+_{j+\frac12}\right)}{a^+_{j+\frac12} - a^-_{j+\frac12}}. \end{aligned} \tag{C.2}$$

We then substitute (C.2) into (2.10) and use the established inequality

$$\overline{h}_j(t) \geq \alpha\left(h^-_{j+\frac12} + h^+_{j-\frac12}\right),$$

where $\alpha = 1/2$ or $1/6$ for $\overline{B}_j$ computed using the trapezoidal or Simpson's rule, respectively, to obtain

$$\overline{h}_j(t+\Delta t) \geq \alpha h^-_{j+\frac12} - \frac{\Delta t}{\Delta x_j}H^{(1)}_{j+\frac12} + \alpha h^+_{j-\frac12} + \frac{\Delta t}{\Delta x_j}H^{(1)}_{j-\frac12}. \tag{C.3}$$

We now consider the first two terms on the RHS of (C.3) and use (C.2) to obtain

$$\alpha h^-_{j+\frac12} - \frac{\Delta t}{\Delta x_j}H^{(1)}_{j+\frac12} = h^-_{j+\frac12}\left[\alpha - \frac{\Delta t}{\Delta x_j}\cdot\frac{a^+_{j+\frac12}\left(u^-_{j+\frac12} - a^-_{j+\frac12}\right)}{a^+_{j+\frac12} - a^-_{j+\frac12}}\right] - \frac{\Delta t}{\Delta x_j}\cdot\frac{h^+_{j+\frac12}a^-_{j+\frac12}\left(a^+_{j+\frac12} - u^+_{j+\frac12}\right)}{a^+_{j+\frac12} - a^-_{j+\frac12}},$$

which is nonnegative provided

$$\Delta t \leq \frac{\alpha\Delta x_j}{a^+_{j+\frac12}},$$

since $a^+_{j+\frac12} - u^+_{j+\frac12} \geq 0$ and $0 \leq u^-_{j+\frac12} - a^-_{j+\frac12} \leq a^+_{j+\frac12} - a^-_{j+\frac12}$.

Similarly, the last two terms on the RHS of (C.3) are nonnegative provided

$$\Delta t \leq -\frac{\alpha\Delta x_j}{a^-_{j-\frac12}},$$

and the proof of the theorem is completed. □

Remark C.2. The proof of Theorem C.1 can be directly extended to the case when the time discretization is performed using the three-stage third-order SSP Runge–Kutta method as it can be written as a convex combination of forward Euler steps.

C.2. Two-dimensional CFL condition

We begin with proving the following lemma.

Lemma C.3. *Assume that in the convex quadrilateral cell $C_{j,k}$, the water depth h is approximated using a nonnegative conservative linear function. Then,*

$$\bar{h}_{j,k}=\frac{1}{2|C_{j,k}|}\Big[r_{j+\frac12,k}\ell_{j+\frac12,k}h^-_{j+\frac12,k}+r_{j-\frac12,k}\ell_{j-\frac12,k}h^+_{j-\frac12,k}+r_{j,k+\frac12}\ell_{j,k+\frac12}h^-_{j,k+\frac12}+r_{j,k-\frac12}\ell_{j,k-\frac12}h^+_{j,k-\frac12}\Big],\tag{C.4}$$

where $r_{j+\frac12,k}$, $r_{j-\frac12,k}$, $r_{j,k+\frac12}$ and $r_{j,k-\frac12}$ are the distances from $\boldsymbol{z}_{j,k}$ to the edges $\boldsymbol{z}_{j+\frac12,k-\frac12}\boldsymbol{z}_{j+\frac12,k+\frac12}$, $\boldsymbol{z}_{j-\frac12,k-\frac12}\boldsymbol{z}_{j-\frac12,k+\frac12}$, $\boldsymbol{z}_{j-\frac12,k+\frac12}\boldsymbol{z}_{j+\frac12,k+\frac12}$ and $\boldsymbol{z}_{j-\frac12,k-\frac12}\boldsymbol{z}_{j+\frac12,k-\frac12}$, respectively.

Proof. We first split the cell $C_{j,k}$ into the following four triangles: $T_{j+\frac12,k}:=\boldsymbol{z}_{j,k}\boldsymbol{z}_{j+\frac12,k+\frac12}\boldsymbol{z}_{j+\frac12,k-\frac12}$, $T_{j-\frac12,k}:=\boldsymbol{z}_{j,k}\boldsymbol{z}_{j-\frac12,k+\frac12}\boldsymbol{z}_{j-\frac12,k-\frac12}$, $T_{j,k+\frac12}:=\boldsymbol{z}_{j,k}\boldsymbol{z}_{j+\frac12,k+\frac12}\boldsymbol{z}_{j-\frac12,k+\frac12}$ and $T_{j,k-\frac12}:=\boldsymbol{z}_{j,k}\boldsymbol{z}_{j+\frac12,k-\frac12}\boldsymbol{z}_{j-\frac12,k-\frac12}$, whose areas are

$$\Big|T_{j\pm\frac12,k}\Big|=\frac12 r_{j\pm\frac12,k}\ell_{j\pm\frac12,k},\quad \Big|T_{j,k\pm\frac12}\Big|=\frac12 r_{j,k\pm\frac12}\ell_{j,k\pm\frac12},\tag{C.5}$$

and

$$|C_{j,k}|=\Big|T_{j+\frac12,k}\Big|+\Big|T_{j-\frac12,k}\Big|+\Big|T_{j,k+\frac12}\Big|+\Big|T_{j,k-\frac12}\Big|.\tag{C.6}$$

We then compute the cell average of h over $C_{j,k}$ and obtain

$$\begin{aligned}\bar{h}_{j,k}&=\frac{\frac{2h^-_{j+\frac12,k}+h_{j,k}}{3}\Big|T_{j+\frac12,k}\Big|+\frac{2h^+_{j-\frac12,k}+h_{j,k}}{3}\Big|T_{j-\frac12,k}\Big|+\frac{2h^-_{j,k+\frac12}+h_{j,k}}{3}\Big|T_{j,k+\frac12}\Big|+\frac{2h^+_{j,k-\frac12}+h_{j,k}}{3}\Big|T_{j,k-\frac12}\Big|}{|C_{j,k}|}\\&\overset{(C.6)}{=}\frac{1}{3|C_{j,k}|}\Big[2\Big|T_{j+\frac12,k}\Big|h^-_{j+\frac12,k}+2\Big|T_{j-\frac12,k}\Big|h^+_{j-\frac12,k}+2\Big|T_{j,k+\frac12}\Big|h^-_{j,k+\frac12}+2\Big|T_{j,k-\frac12}\Big|h^+_{j,k-\frac12}+|C_{j,k}|h_{j,k}\Big].\\&\overset{(C.5)}{=}\frac{1}{3|C_{j,k}|}\Big[r_{j+\frac12,k}\ell_{j+\frac12,k}h^-_{j+\frac12,k}+r_{j-\frac12,k}\ell_{j-\frac12,k}h^+_{j-\frac12,k}+r_{j,k+\frac12}\ell_{j,k+\frac12}h^-_{j,k+\frac12}+r_{j,k-\frac12}\ell_{j,k-\frac12}h^+_{j,k-\frac12}\Big]\\&\quad+\frac13 h_{j,k}.\end{aligned}\tag{C.7}$$

Since $\boldsymbol{z}_{j,k}$ is the geometric center of the quadrilateral and h is a linear function, we have $h_{j,k}=\bar{h}_{j,k}$ and thus (C.7) implies (C.4). □

Equipped with Lemma C.3, we now extend the definition of potentially dry cells as those cells $C_{j,k}$ in which either (2.33), (2.34) or the following inequality:

$$\bar{h}_{j,k}<\frac{1}{2|C_{j,k}|}\Big[r_{j+\frac12,k}\ell_{j+\frac12,k}h^-_{j+\frac12,k}+r_{j-\frac12,k}\ell_{j-\frac12,k}h^+_{j-\frac12,k}+r_{j,k+\frac12}\ell_{j,k+\frac12}h^-_{j,k+\frac12}+r_{j,k-\frac12}\ell_{j,k-\frac12}h^+_{j,k-\frac12}\Big],$$

is satisfied. Recall that in such "dry" cells we reconstruct h instead of w, which ensures that (C.4) is satisfied there. Therefore, we obtain that throughout the entire computational domain

$$\bar{h}_{j,k}\ge\frac{1}{2|C_{j,k}|}\Big[r_{j+\frac12,k}\ell_{j+\frac12,k}h^-_{j+\frac12,k}+r_{j-\frac12,k}\ell_{j-\frac12,k}h^+_{j-\frac12,k}+r_{j,k+\frac12}\ell_{j,k+\frac12}h^-_{j,k+\frac12}+r_{j,k-\frac12}\ell_{j,k-\frac12}h^+_{j,k-\frac12}\Big].\tag{C.8}$$

We now prove the following theorem.

Theorem C.4. *Let h is evolved in time using the forward Euler discretization (2.38). If $\bar{h}_{j,k}(t)\geq 0$ for all j,k, and the time step satisfies the following CFL condition:*

$$\Delta t\leq\frac{1}{2}\min_{j,k}\left\{\frac{r_{j+\frac12,k}}{a^+_{j+\frac12,k}},\frac{r_{j-\frac12,k}}{\left|a^-_{j-\frac12,k}\right|},\frac{r_{j,k+\frac12}}{a^+_{j,k+\frac12}},\frac{r_{j,k-\frac12}}{\left|a^-_{j,k-\frac12}\right|}\right\},$$

then $\bar{h}_{j,k}(t+\Delta t)\geq 0$ for all j,k.

Proof. First, we use (2.24) and rewrite the central-upwind numerical fluxes along the boundaries of $C_{j,k}$ as follows:

$$\begin{aligned}H^{(1)}_{m,i}&=\frac{\ell_{m,i}\Big(n^{(1)}_{m,i}\big[a^+_{m,i}(q^x)^-_{m,i}-a^-_{m,i}(q^x)^+_{m,i}\big]+n^{(2)}_{m,i}\big[a^+_{m,i}(q^y)^-_{m,i}-a^-_{m,i}(q^y)^+_{m,i}\big]+a^+_{m,i}a^-_{m,i}\big[h^+_{m,i}-h^-_{m,i}\big]\Big)}{a^+_{m,i}-a^-_{m,i}}\\&=\frac{\ell_{m,i}\Big(a^+_{m,i}h^-_{m,i}\Big[n^{(1)}_{m,i}u^-_{m,i}+n^{(2)}_{m,i}v^-_{m,i}\Big]-a^-_{m,i}h^+_{m,i}\Big[n^{(1)}_{m,i}u^+_{m,i}+n^{(2)}_{m,i}v^+_{m,i}\Big]+a^+_{m,i}a^-_{m,i}\big[h^+_{m,i}-h^-_{m,i}\big]\Big)}{a^+_{m,i}-a^-_{m,i}}\\&=\frac{\ell_{m,i}\big(h^-_{m,i}a^+_{m,i}\big(\mathcal{V}^-_{m,i}-a^-_{m,i}\big)-h^+_{m,i}a^-_{m,i}\big(\mathcal{V}^+_{m,i}-a^+_{m,i}\big)\big)}{a^+_{m,i}-a^-_{m,i}},\end{aligned}\tag{C.9}$$

where $\mathcal{V}^\pm_{m,i}$ given by (2.37) are the velocities in the direction normal to the corresponding side of $C_{j,k}$. We then substitute (C.9) into (2.38) and use the inequality (C.8) to obtain

$$\begin{aligned}\bar{h}_{j,k}(t+\Delta t)\geq{}&\frac{1}{2|C_{j,k}|}r_{j+\frac12,k}\ell_{j+\frac12,k}h^-_{j+\frac12,k}-\frac{\Delta t}{|C_{j,k}|}H^{(1)}_{j+\frac12,k}+\frac{1}{2|C_{j,k}|}r_{j-\frac12,k}\ell_{j-\frac12,k}h^+_{j-\frac12,k}+\frac{\Delta t}{|C_{j,k}|}H^{(1)}_{j-\frac12,k}\\&+\frac{1}{2|C_{j,k}|}r_{j,k+\frac12}\ell_{j,k+\frac12}h^-_{j,k+\frac12}-\frac{\Delta t}{|C_{j,k}|}H^{(1)}_{j,k+\frac12}+\frac{1}{2|C_{j,k}|}r_{j,k-\frac12}\ell_{j,k-\frac12}h^+_{j,k-\frac12}+\frac{\Delta t}{|C_{j,k}|}H^{(1)}_{j,k-\frac12}.\end{aligned}\tag{C.10}$$

We now consider the first two terms on the RHS of (C.10) and use (C.9) to have

$$\begin{aligned}&\frac{1}{2|C_{j,k}|}r_{j+\frac12,k}\ell_{j+\frac12,k}h^-_{j+\frac12,k}-\frac{\Delta t}{|C_{j,k}|}H^{(1)}_{j+\frac12,k}\\&=\frac{\ell_{j+\frac12,k}h^-_{j+\frac12,k}}{|C_{j,k}|}\left[\frac{r_{j+\frac12,k}}{2}-\frac{a^+_{j+\frac12,k}\Delta t\Big(\mathcal{V}^-_{j+\frac12,k}-a^-_{j+\frac12,k}\Big)}{a^+_{j+\frac12,k}-a^-_{j+\frac12,k}}\right]-\frac{\ell_{j+\frac12,k}h^+_{j+\frac12,k}}{|C_{j,k}|}\cdot\frac{a^-_{j+\frac12,k}\Delta t\Big(a^+_{j+\frac12,k}-\mathcal{V}^+_{j+\frac12,k}\Big)}{a^+_{j+\frac12,k}-a^-_{j+\frac12,k}},\end{aligned}$$

which is nonnegative provided

$$\Delta t\leq\frac{r_{j+\frac12,k}}{2a^+_{j+\frac12,k}},$$

since $a^+_{j+\frac12,k}-\mathcal{V}^+_{j+\frac12,k}\geq 0$ and $0\leq\mathcal{V}^-_{j+\frac12,k}-a^-_{j+\frac12,k}\leq a^+_{j+\frac12,k}-a^-_{j+\frac12,k}$.

Similarly, the third and fourth, the fifth and sixth, and the seventh and eights terms on the RHS of (C.10) are nonnegative provided

$$\Delta t\leq-\frac{r_{j-\frac12,k}}{2a^-_{j-\frac12,k}},\quad\Delta t\leq\frac{r_{j,k+\frac12}}{2a^+_{j,k+\frac12}},\quad\text{and}\quad\Delta t\leq-\frac{r_{j,k-\frac12}}{2a^-_{j,k-\frac12}},$$

respectively, and the proof of the theorem is completed. □

Remark C.5. The proof of Theorem C.4 can be directly extended to the case when the time discretization is performed using the three-stage third-order SSP Runge–Kutta method as it can be written as a convex combination of forward Euler steps.

Acknowledgements. The work of A. Kurganov was supported in part by NSFC grants 11771201, 12111530004 and 12171226, and by the fund of the Guangdong Provincial Key Laboratory of Computational Science and Material Design (No. 2019B030301001).

References

[1] L. Arpaia and M. Ricchiuto, r-adaptation for shallow water flows: conservation, well balancedness, efficiency. *Comput. Fluids* **160** (2018) 175–203.

[2] G. Beckett and J. Mackenzie, Convergence analysis of finite difference approximations on equidistributed grids to a singularly perturbed boundary value problem. *Appl. Numer. Math.* **35** (2000) 87–109.

[3] A. Beljadid, A. Mohammadian and A. Kurganov, Well-balanced positivity preserving cell-vertex central-upwind scheme for shallow water flows. *Comput. Fluids* **136** (2016) 193–206.

[4] A. Bollermann, S. Noelle and M. Lukáčová-Medviďová, Finite volume evolution Galerkin methods for the shallow water equations with dry beds. *Commun. Comput. Phys.* **10** (2011) 371–404.

[5] A. Bollermann, G. Chen, A. Kurganov and S. Noelle, A well-balanced reconstruction of wet/dry fronts for the shallow water equations. *J. Sci. Comput.* **56** (2013) 267–290.

[6] S. Bryson and D. Levy, Balanced central schemes for the shallow water equations on unstructured grids. *SIAM J. Sci. Comput.* **27** (2005) 532–552.

[7] S. Bryson, Y. Epshteyn, A. Kurganov and G. Petrova, Well-balanced positivity preserving central-upwind scheme on triangular grids for the Saint-Venant system. *ESAIM: M2AN* **45** (2011) 423–446.

[8] H. Ceniceros and T. Hou, An efficient dynamically adaptive mesh for potentially singular solutions. *J. Comput. Phys.* **172** (2001) 609–639.

[9] G. Chen, H. Tang and P. Zhang, Second-order accurate Godunov scheme for multicomponent flows on moving triangular meshes. *J. Sci. Comput.* **34** (2008) 64–86.

[10] A. de Saint-Venant, Thèorie du mouvement non-permanent des eaux, avec application aux crues des rivière at à l'introduction des marèes dans leur lit. *C. R. Acad. Sci. Paris* **73** (1871) 147–154.

[11] S. Gottlieb, C. Shu and E. Tadmor, Strong stability-preserving high-order time discretization methods. *SIAM Rev.* **43** (2001) 89–112 (electronic).

[12] S. Gottlieb, D. Ketcheson and C.-W. Shu, Strong Stability Preserving Runge–Kutta and Multistep Time Discretizations. World Scientific Publishing Co. Pte. Ltd., Hackensack, NJ (2011).

[13] W. Huang and R.D. Russell, Adaptive Moving Mesh Methods. Vol. 174 of *Applied Mathematical Sciences*. Springer, New York (2011).

[14] W. Huang and W. Sun, Variational mesh adaptation II: error estimates and monitor functions. *J. Comput. Phys.* **184** (2003) 619–648.

[15] M.E. Hubbard, On the accuracy of one-dimensional models of steady converging/diverging open channel flows. *Int. J. Numer. Methods Fluids* **35** (2001) 785–808.

[16] A. Kurganov, Finite-volume schemes for shallow-water equations. *Acta Numer.* **27** (2018) 289–351.

[17] A. Kurganov and D. Levy, Central-upwind schemes for the Saint-Venant system. *ESAIM: M2AN* **36** (2002) 397–425.

[18] A. Kurganov and G. Petrova, A second-order well-balanced positivity preserving central-upwind scheme for the Saint-Venant system. *Commun. Math. Sci.* **5** (2007) 133–160.

[19] A. Kurganov, Z. Qu, O. Rozanova and T. Wu, Adaptive moving mesh central-upwind schemes for hyperbolic system of PDEs. Applications to compressible Euler equations and granular hydrodynamics. *Commun. Appl. Math. Comput.* **3** (2021) 445–479.

[20] M. Seaïd, Non-oscillatory relaxation methods for the shallow-water equations in one and two space dimensions. *Int. J. Numer. Methods Fluids* **46** (2004) 457–484.

[21] H. Shirkhani, A. Mohammadian, O. Seidou and A. Kurganov, A well-balanced positivity-preserving central-upwind scheme for shallow water equations on unstructured quadrilateral grids. *Comput. Fluids* **126** (2016) 25–40.

[22] H. Tang and T. Tang, Adaptive mesh methods for one- and two-dimensional hyperbolic conservation laws. *SIAM J. Numer. Anal.* **41** (2003) 487–515 (electronic).

[23] A. van Dam and P.A. Zegeling, A robust moving mesh finite volume method applied to 1d hyperbolic conservation laws from magnetohydrodynamics. *J. Comput. Phys.* **216** (2006) 526–546.

[24] Y. Xing, Numerical methods for the nonlinear shallow water equations. In: Handbook of Numerical Methods for Hyperbolic Problems. Vol. 18 of *Handb. Numer. Anal.* Elsevier/North-Holland, Amsterdam (2017) 361–384.

[25] F. Zhou, G. Chen, Y. Huang, J.Z. Yang and H. Feng, An adaptive moving finite volume scheme for modeling flood inundation over dry and complex topography. *Water Resour. Res.* **49** (2013) 1914–1928.

[26] F. Zhou, G. Chen, S. Noelle and H. Guo, A well-balanced stable generalized Riemann problem scheme for shallow water equations using adaptive moving unstructured triangular meshes. *Int. J. Numer. Methods Fluids* **73** (2013) 266–283.

Subscribe to Open (S2O)
A fair and sustainable open access model

This journal is currently published in open access under a Subscribe-to-Open model (S2O). S2O is a transformative model that aims to move subscription journals to open access. Open access is the free, immediate, online availability of research articles combined with the rights to use these articles fully in the digital environment. We are thankful to our subscribers and sponsors for making it possible to publish this journal in open access, free of charge for authors.

Please help to maintain this journal in open access!

Check that your library subscribes to the journal, or make a personal donation to the S2O programme, by contacting subscribers@edpsciences.org

More information, including a list of sponsors and a financial transparency report, available at: https://www.edpsciences.org/en/maths-s2o-programme